Clim Dyn (2010) 34:1015–1039
DOI 10.1007/s00382-009-0619-3

The impact of ENSO periodicity on North Pacific SST variability

Daeho Jin · Ben P. Kirtman

Received: 22 October 2008 / Accepted: 24 June 2009 / Published online: 18 July 2009

Abstract The periodicity of ENSO in nature varies. Here we examine how changes in the frequency of ENSO impacts remote teleconnections in the North Pacific. The numerical experiments presented here are designed to simulate perfectly periodic ENSO in the tropical Pacific, and to enable the air–sea interaction in other regions (i.e., the North Pacific) via a simple mixed layer ocean model. The temporal evolution and spatial structure of the North Pacific SST teleconnection patterns are relatively insensitive to the frequency of ENSO, but the amplitude of the variability is sensitive. Specifically, the 2-year period ENSO experiment (P2) shows weak event-by-event consistency in the ENSO response mature pattern. This is because there is not enough time to damp the previously forced ENSO teleconnections (i.e., 1 year earlier). The 4-year period ENSO experiment (P4) has 1 year damping time before a successive ENSO event matures, so the structure of the response pattern is stably repeated. However, the event-by-event variance of anomaly magnitude, specifically responding to El Niño, is still larger than that in the 6-year ENSO experiment (P6), which has 2-year damping time between consecutive ENSO events. In addition, we tested whether the variability due to tropical remote forcing is linearly independent of the extratropical local variability. Statistical tests indicate that tropical remote forcing can constructively or destructively interfere with local variability in the North Pacific. Lastly, there is a non-linear rectification of the ENSO events that can be detected in the climatology.

Keywords TOGA · Extratropical ENSO responses · ENSO periodicity (frequency) · Tropical–extratropical interaction · Air–sea interaction

D. Jin (✉)
Climate Dynamics Department, George Mason University, Fairfax, VA, USA
e-mail: daehojin@cola.iges.org

Present Address:
D. Jin · B. P. Kirtman
Division of Meteorology and Physical Oceanography, Rosenstiel School of Marine and Atmospheric Science, University of Miami, Miami, FL, USA

B. P. Kirtman
Center for Ocean-Land-Atmosphere Studies, Calverton, MD, USA

1 Introduction

The El Niño-southern oscillation (ENSO) phenomenon impacts global circulation, surface temperatures and rainfall. Between El Niño and subsequent La Niña (or vice versa), the sea surface temperature (SST) difference in the tropical Pacific can be as large as 4°C. This large SST variability impacts the global climate through teleconnections (Liu and Alexander 2007, and references therein). For example, during El Niño events, warm SST anomalies in the tropical Pacific result in local atmospheric response in the form of anomalous convection. This local atmospheric response, in turn, triggers stationary Rossby waves that penetrate into the extratropics, and consequently, tropical remote forcing affects extratropical ocean through air–sea interactions. The wave theory indicates that stationary Rossby waves triggered by tropical heating (or more accurately the sub-tropical decent associated with the heating) emanate from the sub-tropics when mean zonal winds are westerly. The mean westerly wind in the subtropics is stronger in the winter hemisphere than in the summer hemisphere. This along with the fact that the

ENSO events generally mature in boreal winter, suggests that the ENSO forced pattern is stronger in the North Pacific than in the South Pacific (Trenberth et al. 1998).

The periodicity of ENSO varies. For example, Kestin et al. (1998) analyzed the frequency variability of ENSO, and argued that there may be no fixed frequency in nature. Based on observational data, the authors showed that the variability in the 2–3 year spectral range of ENSO decreased between 1920 and 1960. An and Wang (2000) also argued an ENSO frequency change related to the climate shift in mid-1970s (Graham 1994; Trenberth and Hurrell 1994). For example, the authors argued that the ENSO period increased from 2–4 years during 1962–1975 to 4–6 years during 1980–1993. The authors also noted that this ENSO period change is closely related to the structure of coupled mode. In addition, Kim et al. (2003) argued that distinct high frequency and low frequency ENSO modes co-exist, and physical processes and horizontal structures corresponding to the high and low frequency ENSO are fundamentally different from each other.

Experimental results also support the notion of a changing frequency for ENSO. Toniazzo (2006) analyzed ENSO variability of the Hadley Centre Coupled Ocean-Atmosphere GCM (HadCM3) in three stable climate regimes: Last Glacial Maximum, pre-industrial period, and greenhouse stabilization scenario. The author argued that the period of the oscillation becomes shorter from the past to the future. However, the relationship between global warming and the ENSO frequency is still an open question. For example, Zelle et al. (2005) showed that there are no significant changes in the ENSO period when the global mean surface temperature increased.

The changing frequency of ENSO has been studied from many different perspectives. However, the sensitivity of remote teleconnections in response to changes in the ENSO frequency has not been examined. In the North Pacific, for example, we might expect the remote response to be sensitive to the frequency of ENSO. If ENSO triggers or forces some response in the North Pacific, we expect this response to have a life cycle and time scale that is due, in part, to local processes (i.e., coupled feedbacks, wave dynamics, damping, etc.). In turn, if the ENSO life cycle is fast compared to the local North Pacific life cycle, we might expect constructive or destructive interference. Conversely, if the ENSO life cycle is relatively long then the character of the interference may be considerably different. The purpose of this study is to examine how the frequency of ENSO impacts the extratropics, specifically in the North Pacific where the effect of ENSO is clearly seen. For this study we developed a modeling strategy where the periodicity of ENSO can be completely specified. This experimental design makes it possible for us to assess and compare the effect of different ENSO frequencies on the remote teleconnections in the North Pacific. There is an interesting by-product of this experimental design, namely the experiments can be used to estimate the decay time of the forced response in the North Pacific.

In the next section, the detailed experimental design is described. In the third section, the composite analysis of surface temperature in the North Pacific is discussed. In the forth section, a relationship between local and remote forcing is analyzed. A comparison to the observational estimates is displayed in the fifth section, and changed climatology due to tropical ENSO forcing is examined in the sixth section. Conclusions are given in the last section.

2 Numerical model and experimental design

The model is composed of atmospheric general circulation model (AGCM), tropical Pacific prescribed sea surface temperature (SST) as a lower boundary condition, and simple slab mixed-layer ocean model coupled to AGCM outside of tropical Pacific. For the AGCM, we use the National Center for Atmospheric Research (NCAR) Community Atmosphere Model Version 3 (CAM3) with a horizontal resolution of T42 and 26 vertical levels with a hybrid terrain-following coordinate. The dynamical core is Eulerian spectral and originated from NCAR CCM3 (Kiehl et al. 1998), and the changes are described in Collins et al. (2006). The mixed-layer ocean model coupled to AGCM is a simple thermodynamic slab mixed-layer model which is part of the CAM3/CCSM3 modeling system. The depth of mixed-layer is fixed to the climatological annual cycle with a 200 m cap.

ENSO forcing in the tropical Pacific is prescribed as a lower boundary condition to the AGCM. The prescribed region is defined as 120°E–85°W in longitude and 20°S–20°N (M20) in latitude. The prescribed SST data is composed of a climatological annual cycle and ENSO composite anomalies, which are obtained from the Hadley Center SST dataset (Rayner et al. 2000). The climatological annual cycle is formed from monthly mean from January 1949 to December 1998. The selection criterion for the ENSO composite anomalies is based on the NINO3.4 index (area average of SST for 5°S–5°N, 170–120°W) so that the top 9 January NINO3.4 values define the warm event composites and the bottom 9 January NINO3.4 values define the cold event composites. We have excluded the 1968–1969, 1986–1987, and 1987–1988 events even though they meet our composite criterion. The reason for this is because these events have significantly different evolutions (i.e. they do not peak in boreal winter). See Table 1 for a list of events contributing to the composites.

In the control experiment, only the climatological annual cycle is used for the tropical prescribed forcing

Table 1 For the ENSO composite analysis, nine El Niño and nine La Niña events are selected based on Jan(1) NINO3.4

	Years				
El Niño	1957–1958	1963–1964	1965–1966	1972–1973	1982–1983
	1991–1992	1994–1995	1997–1998	2002–2003	
La Niña	1949–1950	1955–1956	1970–1971	1973–1974	1975–1976
	1984–1985	1988–1989	1998–1999	1999–2000	

The years during which the peak is not located in boreal winter are excluded

whereas, in the ENSO experiment, the ENSO composite anomalies are added to the climatological annual cycle with fixed period. There is an important subtlety in the control simulations that should be noted. In the control (like the ENSO experiments) the SST is prescribed in the tropical Pacific, except it is specified as climatology. The reason we have chosen to perform the control simulation in this manner is to be as consistent with the ENSO experiments as possible. In other words, the same energetic inconsistencies in the ENSO experiments in the prescribed SST region are also present in the control simulations.

In addition, we argue that the perfectly periodic ENSO can reduce the uncertainties in ENSO teleconnections that are due to vagaries in the ENSO itself. In this study, the period of ENSO is set as 2, 4, or 6 years (Fig. 1). There is an important point to note in Fig. 1. The duration of the warm and cold periods does not change from experiment to experiment. The only difference among the experiments is the time in between warm and cold events. This strategy is used because (1) we want to keep the evolution of ENSO similar to nature, and (2) we want to examine a decaying time scale of extratropical ENSO response. On the other hand, there is a potential problem with this experimental design. As mentioned in the introduction section, tropical Pacific SST structures corresponding to the high and low frequency ENSO could be different in nature (e.g. An and Wang 2000; Kim et al. 2003). In this study, this SST structure problem is simplified by using the ENSO composite mean structure mentioned above. This strategy enables us to focus on the life cycle of extratropical ENSO responses.

The total simulated period of each experiment is 72 years, but only the last 60 years are used for analysis. The set of experiments are summarized in Table 2. In addition, we note that the number after the name of month represents the simulation year. For example, "JAN 1" or "JAN(1)" means "January of year 1."

Lastly, the surface temperature and geopotential height at 500 hPa for the regression analysis in Sect. 3.2 is from the National Centers for Environmental Prediction–National Center for Atmospheric Research (NCEP–NCAR) reanalysis dataset (Kalnay et al. 1996). The horizontal resolution is 2.5° latitude by 2.5° longitude. The SST data for the Sect. 5 is from the Hadley Center SST dataset (Rayner et al. 2000). The horizontal resolution is 1° by 1°. The period of both datasets used in this study is from January 1950 to December 2004. In this study, all anomalies are calculated by removing 20 year running mean annual cycle. This approach is used to remove very low frequency variability (i.e., trend).

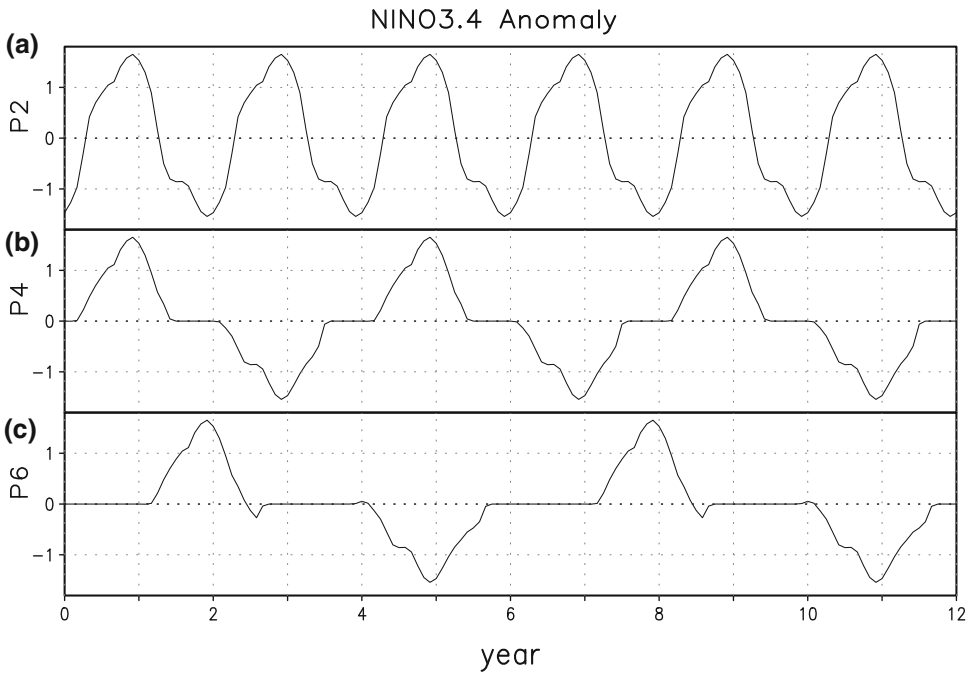

Fig. 1 NINO3.4 index (area average of surface temperature, 5°S–5°N, 170–120°W) anomaly in the (**a**) 2 year period, (**b**) 4 year period, and (**c**) 6 year period ENSO experiment. Anomaly is a deviation from the control experiment annual cycle

Table 2 A set of experiments is described

Prescribed SST (20°S–20°N)	Experiment	Duration/cycle
Annual cycle only	(M20)Ctl	60 years/60 cyc
ENSO Period		
2 years	(M20)P2	60 years/30 cyc
4 years	(M20)P4	60 years/15 cyc
6 years	(M20)P6	60 years/10 cyc

The longitudinal definition of prescribed region is commonly from 120°E to 85°W

3 The ENSO composite analysis of surface temperature

3.1 Temporal evolution of ENSO responses: meridional mean composite in the North Pacific

In this study, the temporal and structural evolution of individual ENSO events in the tropical Pacific is the same among different ENSO period experiments. The durations of the warm and cold periods are the same, and the only difference is in the time between events. Hence, we can simply investigate the effect of ENSO periodicity by comparing the ENSO forced patterns in different ENSO period experiments. In this section, we compare the life cycle and time scale of ENSO forced patterns through time-longitude cross-sections.

Figure 2 shows time-longitude cross-sections of the surface temperature composite in the North Pacific basin. The anomaly defined here is the deviation from the control experiment annual cycle, and the surface temperature is meridionally averaged from 40 to 50°N,[1] which is determined from the structures of the El Niño and La Niña responses which will be discussed in Sect. 3.2. All three experiments in Fig. 2 share common features such as a maximum response in boreal spring to summer. In boreal spring following the El Niño peak, the positive anomaly around 130°W is also quite similar among the experiments. All three experiments indicate that the negative SSTA in the central North Pacific in response to the El Niño forcing is stronger than the positive SSTA response to the La Niña forcing. In the case of the P6 experiment, the anomalies associated with the El Niño forced pattern are only slightly stronger than that of the La Niña forced pattern.

The atmospheric response to ENSO in the Northern Hemisphere is typically a stationary wave train from the North Pacific to the North Atlantic (Trenberth et al. 1998, and references therein.). The effect of ENSO SSTA in the "perfectly periodic ENSO" framework (i.e., the ENSO experiment composite minus the control experiment climatology) is also a wave train pattern (Jin and Kirtman 2009). For example, in the case of El Niño, geopotential height (GPH) at 510 hPa indicates a negative anomaly in the central North Pacific basin, and positive anomaly over Canada in boreal winter season. In addition, Jin and Kirtman (2009, manuscript submitted to *J Geophys Res*) argued that surface wind anomaly responding to El Niño in boreal winter is a cyclonic circulation in central to northeastern North Pacific. This cyclonic circulation results in increased latent and sensible heat flux anomaly from sea surface to atmosphere in the central mid-latitude North Pacific, and decreased heat flux anomaly around western Canadian coast. As a result, central negative and northeastern positive SSTA occurs one season later (i.e., boreal spring), as shown in Fig. 2. In contrast to the El Niño responses, the La Niña forced wave train pattern is fairly weak (Jin and Kirtman 2009). Jin and Kirtman (2009) showed that the magnitude of anomalous vertical wind in the tropical Pacific is weaker than that in El Niño. The Pacific basin zonal mean atmospheric meridional circulation in response to La Niña indicates that mid-latitude atmosphere is similarly upward as the El Niño response. Accordingly, the GPH anomaly at 510 hPa shows significantly different pattern from conventional wisdom (i.e., similar pattern with opposite sign to the El Niño responses). For example, there are negative anomalies in western mid-latitude North Pacific, and positive anomalies in the Arctic region around Bering straight. Surface heat flux anomalies and corresponding SST responses are also weaker compared to the El Niño events (Jin and Kirtman 2009, manuscript submitted to *J Geophys Res*).

In addition to the common features among the experiments, notable differences are also seen. First, the details of the ENSO forced pattern in the central North Pacific are different. For example, after the El Niño events, the negative anomalies in the P2 experiment are broader in longitudes, but weaker than those in the P4 experiment. Moreover, in the case of the P4 and P6 experiments, the lingering pattern (i.e., the response in the North Pacific which persists beyond the life cycle of the tropical ENSO forcing, typically a year after the ENSO peak), is also different. In the P4 experiment, the same sign anomalies persist in the similar longitudes from the ENSO mature season to 1 year after the ENSO decay season. However, in the P6 experiment, the lingering pattern 1 year after the ENSO event is shifted eastward. (Details are discussed in the Sect. 3.2).

In Fig. 3, the anomalies are calculated using the climatology from the corresponding experiment (e.g., use the P4 mean annual cycle for calculating the P4 anomalies) as opposed to the control experiment annual cycle. In

[1] We also tested a domain of meridional mean, 35–55°N, but there are only minor differences from the domain from 40–50°N.

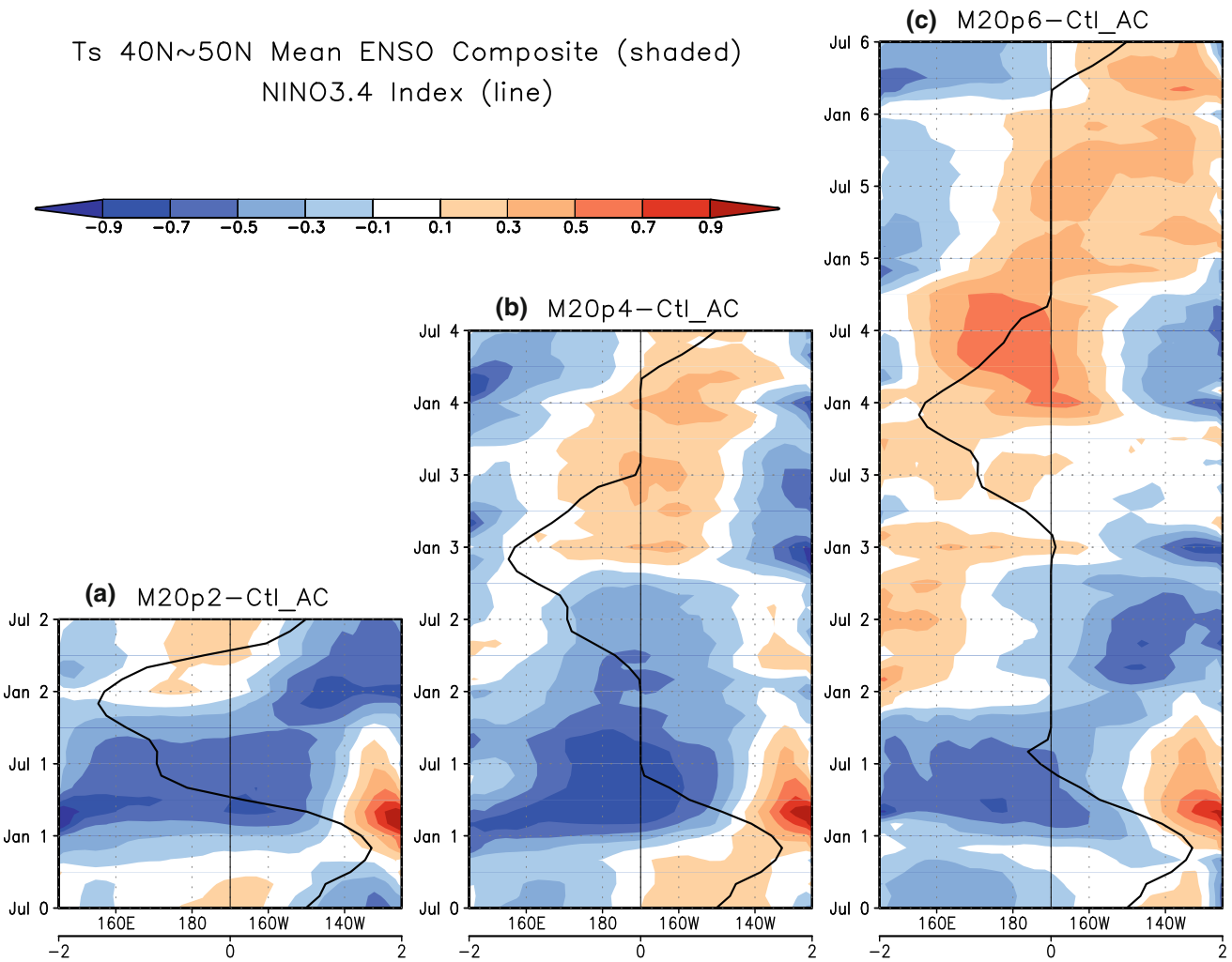

Fig. 2 Meridional mean (40–50°N) ENSO composite evolution of surface temperature anomalies (°C, *shaded*) and NINO3.4 index evolution (°C, *line*) in the (**a**) P2, (**b**) P4, and (**c**) P6 experiment. The anomaly is a deviation from the control experiment annual cycle (Ctl_AC). The *numbers after month* indicate year. Hence, "Jul 0" means July in year 0. Because the tropical ENSO forcing is perfectly periodic, "Jul 2" in (**a**), for example, is same to "Jul 0" in the bottom, so on

contrast to Fig. 2, Fig. 3 shows more symmetric El Niño and La Niña forced patterns with opposite sign. The lingering patterns after the El Niño and La Niña events are also similar with opposite sign in the P4 and P6 experiments. Of course, the lingering patterns in the P4 experiment are different from those in the P6 experiment, consistent with the results of Fig. 2. The occurrence of a similar pattern with opposite sign (Fig. 3) versus totally different patterns (Fig. 2) between the El Niño and La Niña forced signals is reminiscent of the issue of the nonlinear ENSO response (Hoerling et al. 1997, 2001). Hoerling et al. (1997) argued that the ENSO response in the North Pacific is not merely of the opposite sign with same pattern, but is zonally or meridionally shifted with different amplitude, or totally different patterns (i.e. nonlinear ENSO response). These nonlinear ENSO responses in respect to the control experiment climatology result in modified climatology in the ENSO experiments,[2] which is discussed in the Sect. 6.

3.2 Spatial structure of the seasonal ENSO responses

Previously, we compared the temporal evolution of North Pacific SST in response to the ENSO events of differing periodicity. Generally speaking, the temporal evolution of North Pacific SST among the experiments is similar, but the details of the structure are different. In order to closely examine the differences in spatial structure, the seasonal

[2] The climatologies in the P2, P4, and P6 experiments are different from each other, which is consistent with the argument that the details of ENSO forced patterns in each experiment are different. However, the differences among the P2, P4 and P6 experiments are not large as those between the ENSO experiment (e.g., P2, P4 or P6) and control run.

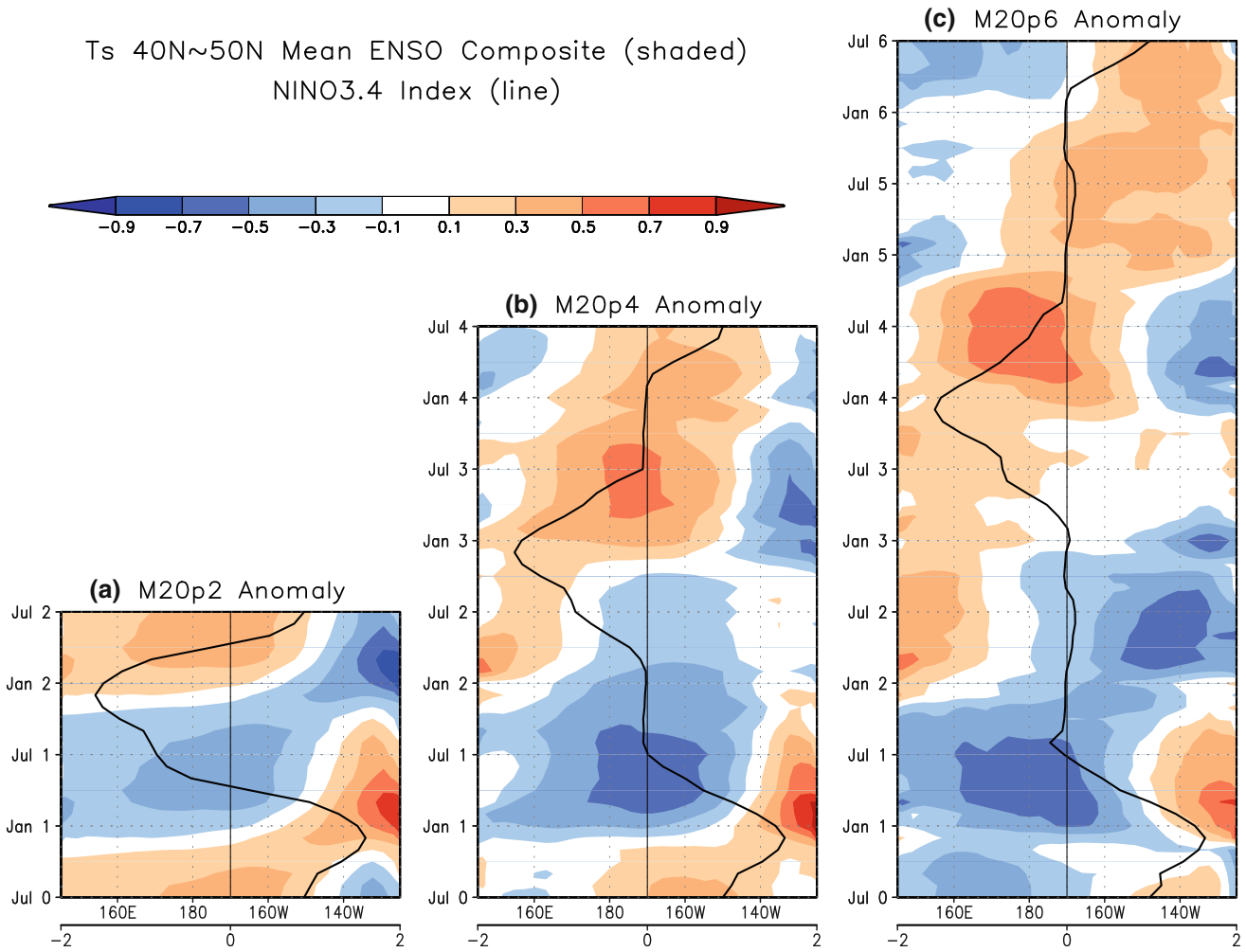

Fig. 3 Same as Fig. 2, but the anomaly is from own annual cycle of each experiment

mean surface temperature ENSO composite pattern is shown in Figs. 4 and 5.

In the case of the El Niño composite (Fig. 4), the temporal evolution and general features such as the cold anomalies in the central North Pacific are similar among the experiments, but important details among the experiments are also apparent. For instance, the spatial correlation coefficient in Table 3 indicates that each pattern is over 83% similar in boreal spring to summer when the El Niño forced pattern matures in the North Pacific. The spatial patterns of the P2 and P4 experiments are even more similar (92–94%), and the P6 experiment is slightly different from the other experiments (83–88%, and the significance of calculation is discussed in the Appendix). Generally, these results are consistent with the time-longitude cross-section figures discussed earlier.

The El Niño anomaly composite patterns (Fig. 4 shaded) are similar between the P2 and P4 experiments, but standardized composite patterns (Fig. 4 contour) are different. Here, the standardization is calculated by dividing the anomaly composite with the standard deviation of the anomaly.[3] In the boreal spring season when the El Niño responses are the strongest, the P4 and P6 experiments show standardized anomalies that are lower than -1.5 although the location of the lowest anomaly is different between them. In contrast, the P2 experiment shows normalized anomalies under -1.0, but not lower than -1.5 in the eastern mid-latitudes. Because the normalized anomaly difference (<-1.0 vs. <-1.5) is larger than the composite mean anomaly difference (<-0.9 vs. <-1.1°C), we can deduce that the standard deviation, i.e. the event-to-event variation in the P2 experiment, is bigger than the other experiments.

In the case of La Niña (Fig. 5), the composite pattern similarity among the experiments decreases compared to the El Niño events. For example, the P2 experiment is

[3] In the case of P2 experiment, for example, there are 30 samples to calculate the standard deviation due to 2 year period for 60 simulation years. In the same way, the P4 experiment has 15 samples, and the P6 experiment has 10 samples for the composite.

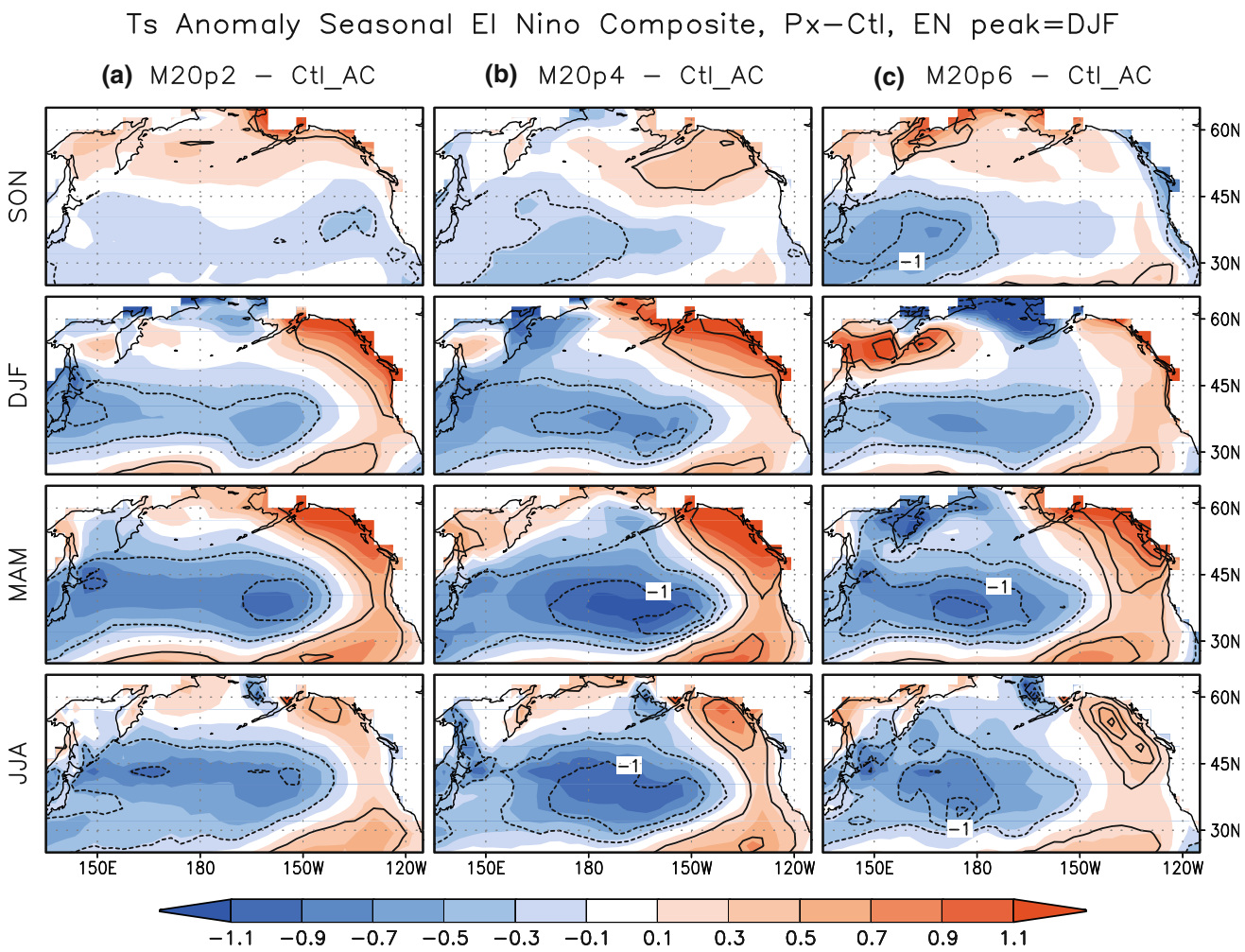

Fig. 4 Seasonal surface temperature El Niño composite (*shading*), and standardized composite (*contour*) in the (**a**) P2, (**b**) P4, and (**c**) P6 experiment. Anomalies are from the control experiment annual cycle. The peak of El Niño is in December–February, second panels from the top. The standardization is calculated by dividing the anomaly composite with the standard deviation of the anomaly used in the composite analysis. *Solid line* indicates positive, and *dash line* indicates negative values. *Zero line* is suppressed. Contour level is 0.5. The unit for the surface temperature anomaly composite is °C

considerably different from the other experiments (see Table 3). The differences between the P2 experiment and other experiments are apparent in boreal fall, one season before the La Niña peak. In boreal fall, there are broad negative anomalies around 40°N in the P2 experiment, which look similar to the El Niño forced pattern in Fig. 4. Because the remote ENSO forcing in the P2 experiment exists every year, the top panel of Fig. 5a is actually a residual of the El Niño forced pattern. On the other hand, in the P4 or P6 experiment, there are weak or no negative anomalies around 40°N. This is because the residual of the El Niño forced pattern is damped by local processes for another year (in the P4 experiment) or 2 years (in the P6 experiment) before ENSO changes phase and new forcing emerges from the tropics.

The latent and sensible heat flux forcing in response to La Niña in the North Pacific is apparently seen in the late fall to early winter season, just before the La Niña peak season (Jin and Kirtman 2009, manuscript submitted to *J Geophys Res*). Figure 6 shows La Niña composite surface latent and sensible heat flux anomaly in this season (i.e., November–December). The heat flux anomaly patterns are qualitatively similar among the experiments. For example, all experiments simulate a central Pacific negative anomaly and eastern Pacific positive anomaly although the details such as magnitude and peak location are different. Relatively weak negative anomaly in the central North Pacific in the P2 experiment is reasonable if the previous SSTA pattern is considered. As mentioned above, Fig. 5a top panel shows a negative anomaly in the central North Pacific as a residual of the El Niño responses. Negative SSTA produces positive heat flux anomaly (i.e., heat flux from atmosphere to sea surface) due to negative feedback by local air–sea interaction. Hence positive heat flux by

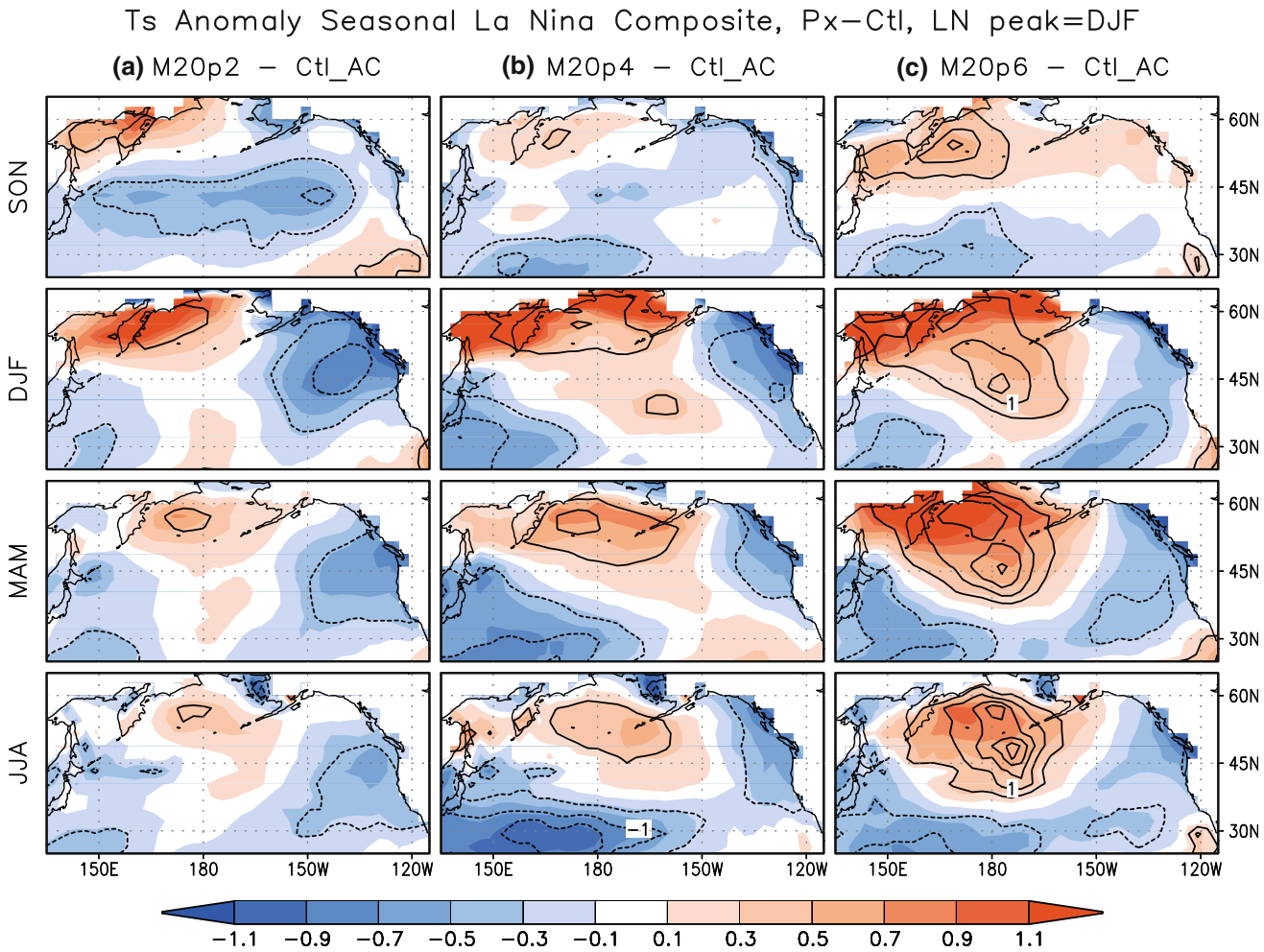

Fig. 5 Same as Fig. 4, but for the La Niña composite

local damping can weaken the negative heat flux in response to the tropical La Niña forcing.

As a result, a positive SSTA response in the central North Pacific is seen in the P4 and P6 experiments, but the response is weak in the P2 experiment (Fig. 5). Generally, the larger magnitude of the negative SST anomaly in boreal fall leads to the smaller positive SSTA response to La Niña in the subsequent spring season in the central North Pacific. It is also worth noting that, from boreal spring to summer after the La Niña peak season, the magnitude of the standardized SSTA pattern is different between the P4 and P6 experiment. The robust La Niña response in the P4 experiment is associated with the negative anomaly in the western mid-latitude North Pacific, while the P6 experiment simulates a stable positive anomaly response in the central high-latitude North Pacific.

Overall, the tropical La Niña SST forcing is same, and remote heat flux forcing in the North Pacific is qualitatively similar, but the La Niña response patterns are different. This is largely due to the different SSTA pattern in the North Pacific before the La Niña peak season. Essentially, the response in the North Pacific is due to the several competing factors, but can be boiled down to the time between ENSO events (i.e., remote forcing) and the local damping time scale of the response (i.e., strength of local coupled feedbacks).

In principle, the same mechanism or competition should be applied to the El Niño composite shown in Fig. 4. However, the top panel of Fig. 4a is not qualitatively different from Fig. 4b, c. This is because the La Niña response in the P2 experiment is relatively weak compared to the El Niño response, and, in turn, because the residual of the La Niña response is also weak when tropical El Niño forcing is about to emerge. In the bottom panel of Fig. 5a, the anomalies in the central North Pacific are hardly detected in current shading levels. Therefore the El Niño response in the P2 experiment remains quite similar to the P4 or P6 experiments. Based on the same argument as with the La Niña composite, we can deduce that the differences in the details of the El Niño forced response among experiments

Table 3 ENSO composite seasonal mean spatial correlation between the ENSO experiments calculated in 145°E–125°W, 30–60°N. Spatial patterns are shown in Figs. 4 and 5. The significance of correlation is discussed in Appendix

	Season	P2 vs. P4	P2 vs. P6	P4 vs. P6
El Niño Composite (Peak=DJF)	Sep-Oct-Nov	0.633	0.359	0.592
	Dec-Jan-Feb	0.922	0.732	0.568
	Mar-Apr-May	0.926	0.880	0.830
	Jun-Jul-Aug	0.943	0.843	0.839
La Niña Composite (Peak=DJF)	Sep-Oct-Nov	0.501	0.310	0.428
	Dec-Jan-Feb	0.761	0.768	0.899
	Mar-Apr-May	0.640	0.757	0.786
	Jun-Jul-Aug	0.555	0.731	0.840

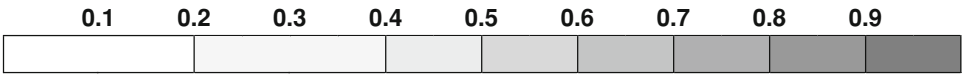

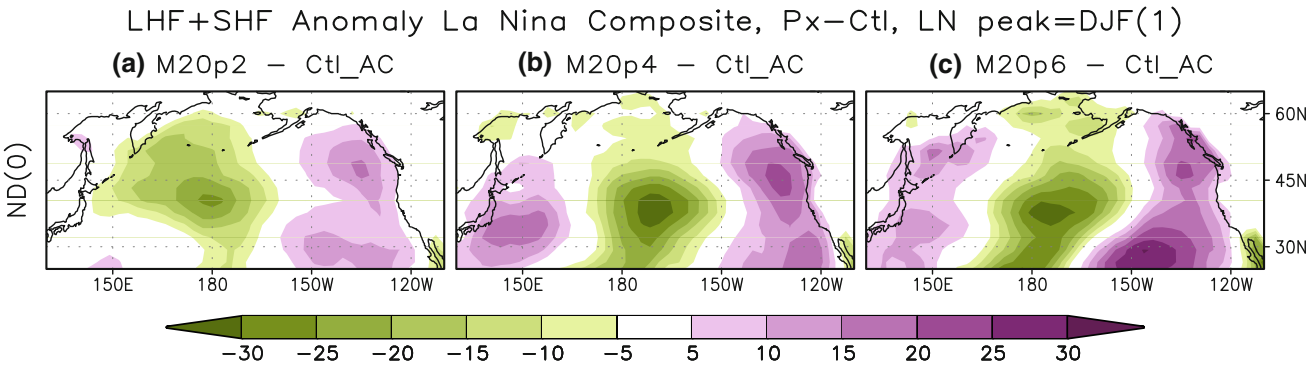

Fig. 6 November–December La Niña composite of latent and sensible heat flux anomaly in the (**a**) P2, (**b**) P4, and (**c**) P6 experiment. Anomalies are from the control experiment annual cycle. The peak of La Niña is in December–February, just after the composite months. The unit is W m^{-2}

are due to the differences in the details of initial surface temperature pattern in the developing phase of El Niño, with an assumption that surface heat flux in response to El Niño is qualitatively similar, which may hint at some potential predictability for the North Pacific SST.

In addition to the ENSO response pattern, the previous analysis noted that the El Niño lingering patterns, which appear 1 year after the peak of El Niño in the P4 and P6 experiments, are different. It was noted that the Center of the lingering pattern after the El Niño in the P6 experiment is shifted eastward while that in the P4 experiment remains fixed in longitude. In Fig. 7 top panels which show boreal fall composite, three seasons after the peak of El Niño, the maximum anomaly from the control experiment which is located in the central North Pacific is over 0.7°C in the P4 experiment, while it is not more than 0.5°C in the P6 experiment. Stronger signals in the P4 experiment remain in nearly the same location until the next boreal summer season (JJA(2) in Fig. 7a). In the P6 experiment, the negative anomalies are dissipated in the boreal winter season (DJF(2) in Fig. 7b), and new negative anomalies in the eastern North Pacific (ENP) develop at the same time. This negative anomaly is the strongest around the boreal spring season. In spite of these differences, statistical t-tests indicate that the P4 and P6 experiments are not significantly different at 90% significance level in the boreal spring (MAM(2)) and summer (JJA(2)) seasons. The ENP negative anomaly shown as a lingering pattern after El Niño in the P6 experiment is barely related to El Niño as discussed below.

In order to examine the pattern most related to the ENP SSTA, we performed a lag-lead regression analysis. First, we build an area average time series in 155–140°W, 40–50°N, representing the ENP SSTA (i.e., ENP index). Then we calculated the surface temperature (Ts) and geopotential height at 500 hPa (GPH500) patterns regressed onto the ENP index (Fig. 8). Previously in Fig. 7, the ENP SSTA is of maximum magnitude in boreal spring, five

seasons after the El Niño peak season. Hence we calculated 15 months lagged regression pattern (i.e., Ts and GPH500 lead ENP index by 15 months) shown in Fig. 8a. In the P6 experiment (left column) and observational estimates (right column), El Niño-like Ts pattern is detected in the tropical Pacific. However, the magnitude of positive anomaly is weak (0.2–0.3°C/°C in the P6 experiment, and 0.4–0.5°C/°C in the observational estimates). If we consider variability of ENP index, the standard deviation of which is overall 0.7°C (maximum 1°C in the spring season) in the P6 experiment, and overall 0.4°C (maximum 0.6°C in the fall season) in the observational estimates, the relationship with El Niño is weak.

Moreover, Ts and GPH500 regression patterns are nearly the same between the P6 and control experiments. This also suggests that ENSO is not related to the ENP index. Because the control experiment has only climatological annual cycle in the tropical Pacific, we think that the development of negative ENP SSTA is due to local forcing such as internal atmospheric dynamics. Observational estimates in Fig. 8c hints that a stationary wave train can be responsible for the ENP SSTA variation. Additional

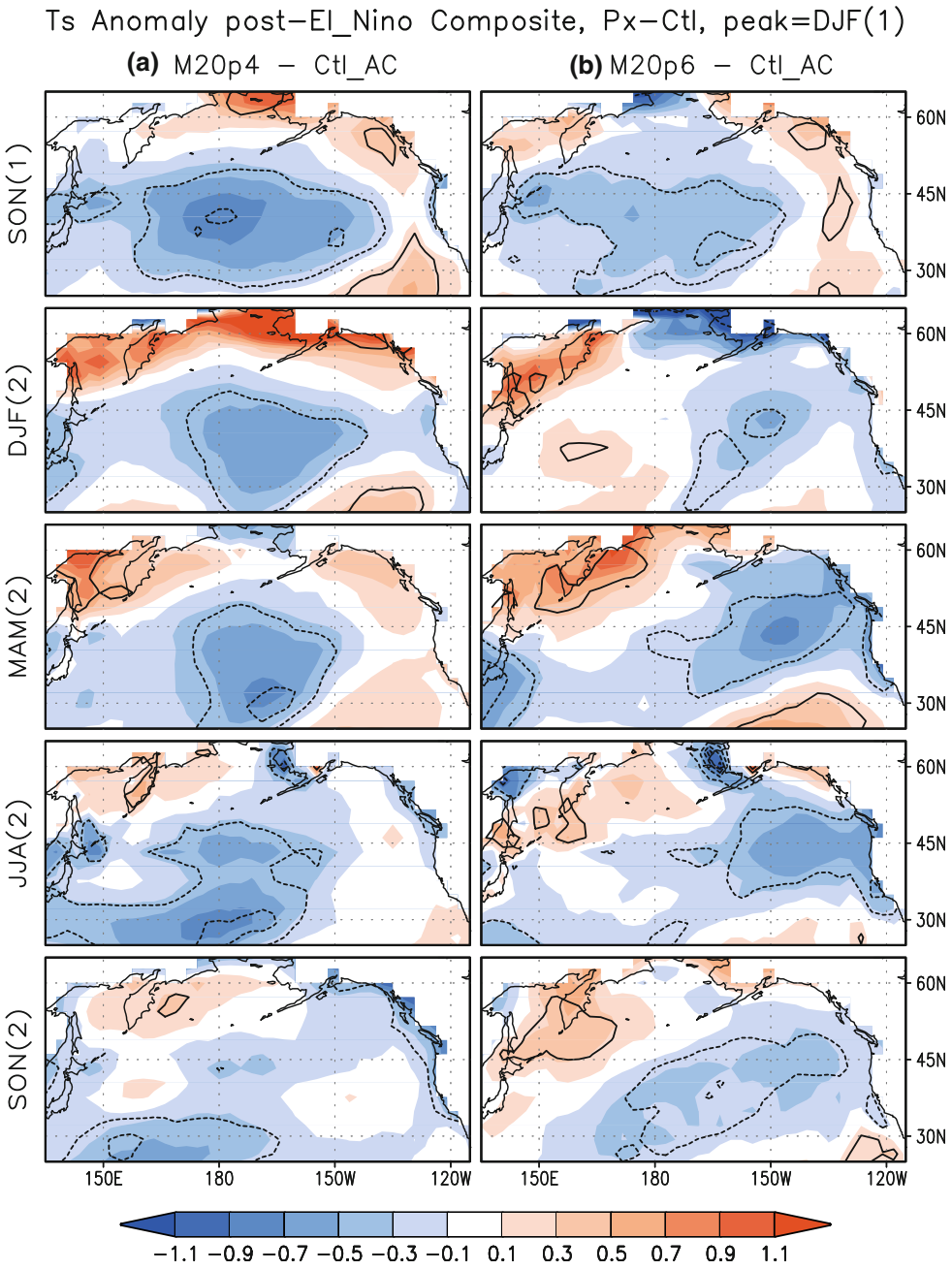

Fig. 7 Same as Fig. 4, but 1 year later in the case of (**a**) P4 and (**b**) P6 experiment. The peak of El Niño was in December–February in previous year (DJF(1))

regression analyses of surface pressure and near-surface wind indicate that, common in all the experimental results and the observational estimates, surface pressure regressed pattern is also of negative anomaly in just south of Alaska (i.e. barotropic system), and near-surface wind is cyclonic (not shown here). As a part of cyclonic system, winds blown from Bering strait to the ENP area take heat from the sea surface to the atmosphere.

Compared to the lingering pattern after the El Niño event, the pattern after the La Niña event is not much different between the P4 and P6 experiments. Figure 9 shows that both experiments have similar structure with positive anomalies in the northern central-to-east Pacific and negative anomalies in the west-to-central Pacific around 30°N. The Center of the northern positive anomaly is shifted eastward after boreal winter, 1 year after the La Niña in the both experiments. Although the details of anomaly pattern are different among the experiments, the north and south dipole pattern typically remains during the year after the La Niña. In the case of standardized pattern, the P6 experiment shows more robust signals in boreal fall (SON(1) in Fig. 9b), three seasons after the La Niña peak season continued from Fig. 5c bottom panel. However, robust positive signals in the northern North Pacific weaken in following winter, and thereafter they become similar to those in the P4 experiment (MAM(2) in Fig. 9a, b). This result suggests that robust La Niña response signals in the central North Pacific are not maintained over 1 year.

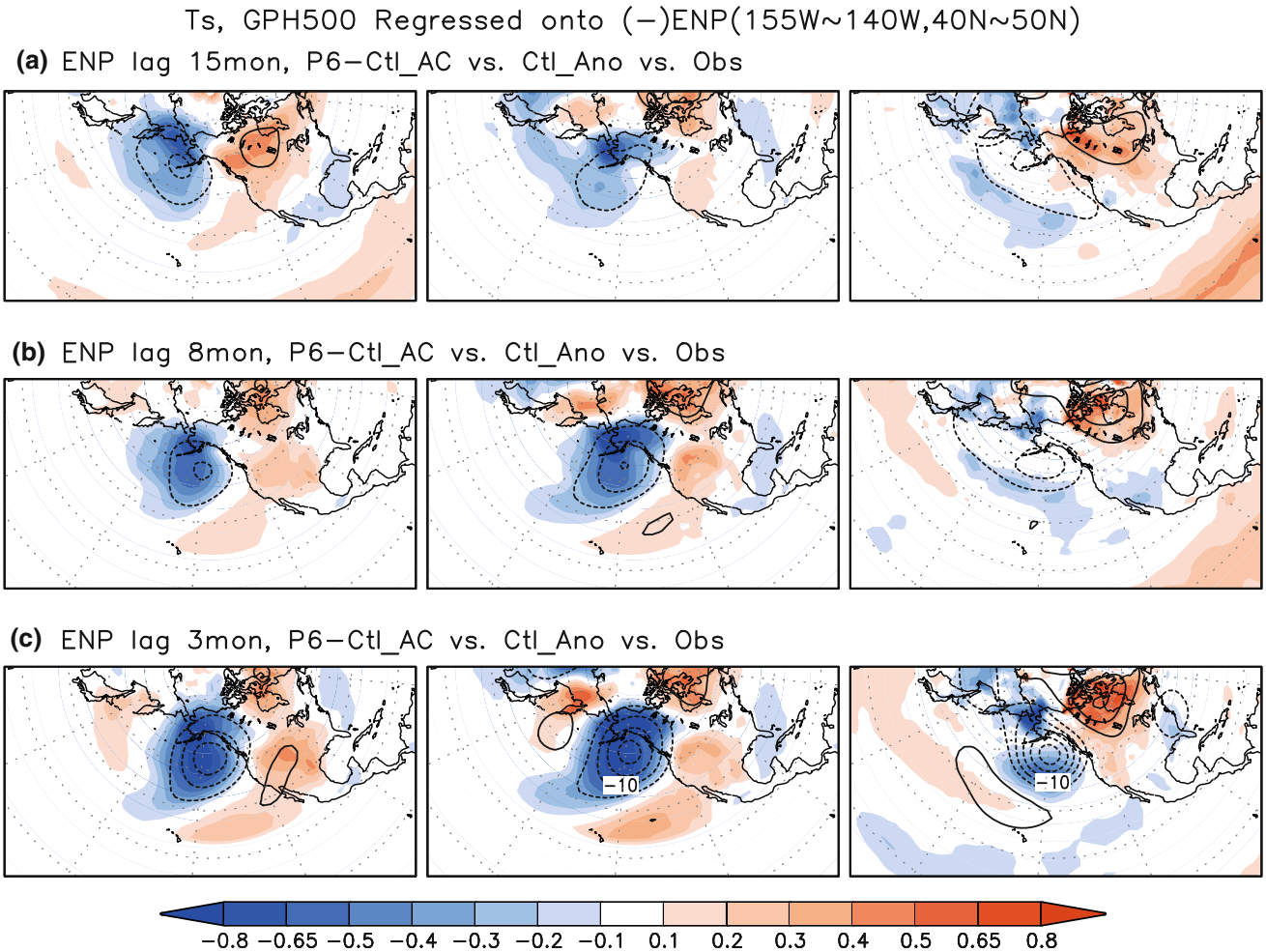

Fig. 8 Surface temperature (Ts, *shaded*) and geopotential height at 500 hPa (GPH500, *contour*) are regressed onto the ENP index which is area average time series for Ts in 155–140°W, 40–50°N. The regression pattern shown here is for the negative ENP index. (**a**) ENP lags 15 months behind Ts and GPH500, (**b**) ENP lags 8 months, and (**c**) ENP lags 3 months. *Left column* is in the case of P6 experiment anomaly from control experiment annual cycle, *center column* is of the control experiment anomaly, and *right column* is for the observational estimates (NCEP-NCAR reanalysis dataset). *Solid line* indicates positive values, and *dash line* indicates negative values. *Zero line* is suppressed. Contour level is 5 m/°C. The unit for Ts is °C/°C, and for GPH500 is m/°C

4 Competition between local and remote forcing

As previously shown, standard deviation of composite anomaly is usually as large as anomaly composite itself despite of the same ENSO forcing repeating again and again. This variation is caused by several factors, and one of them is the competition between atmospheric internal dynamics (i.e., local forcing) and the effect of ENSO (i.e., remote forcing). Related to this competition, Yeh and Kirtman (2004) actively controlled the atmospheric variability coupled to the ocean by use of the interactive ensemble strategy (Kirtman and Shukla 2002), and argued that the tropical remote forcing is easier to detect as the atmospheric stochastic forcing of the ocean decreases. In this study, we control the tropical remote forcing as opposed to the atmospheric noise due to internal dynamics. Because the tropical ENSO forcing is perfectly periodic in this study, the ENSO forced pattern in the North Pacific is expected to be periodic (or quasi-periodic). In this section, we examine the relationship between local and remote forcing in aspects of pattern consistency and any variance change due to the addition of remote forcing. First, we will examine ENSO response pattern similarity in the same season between any two ENSO events. If the effect of

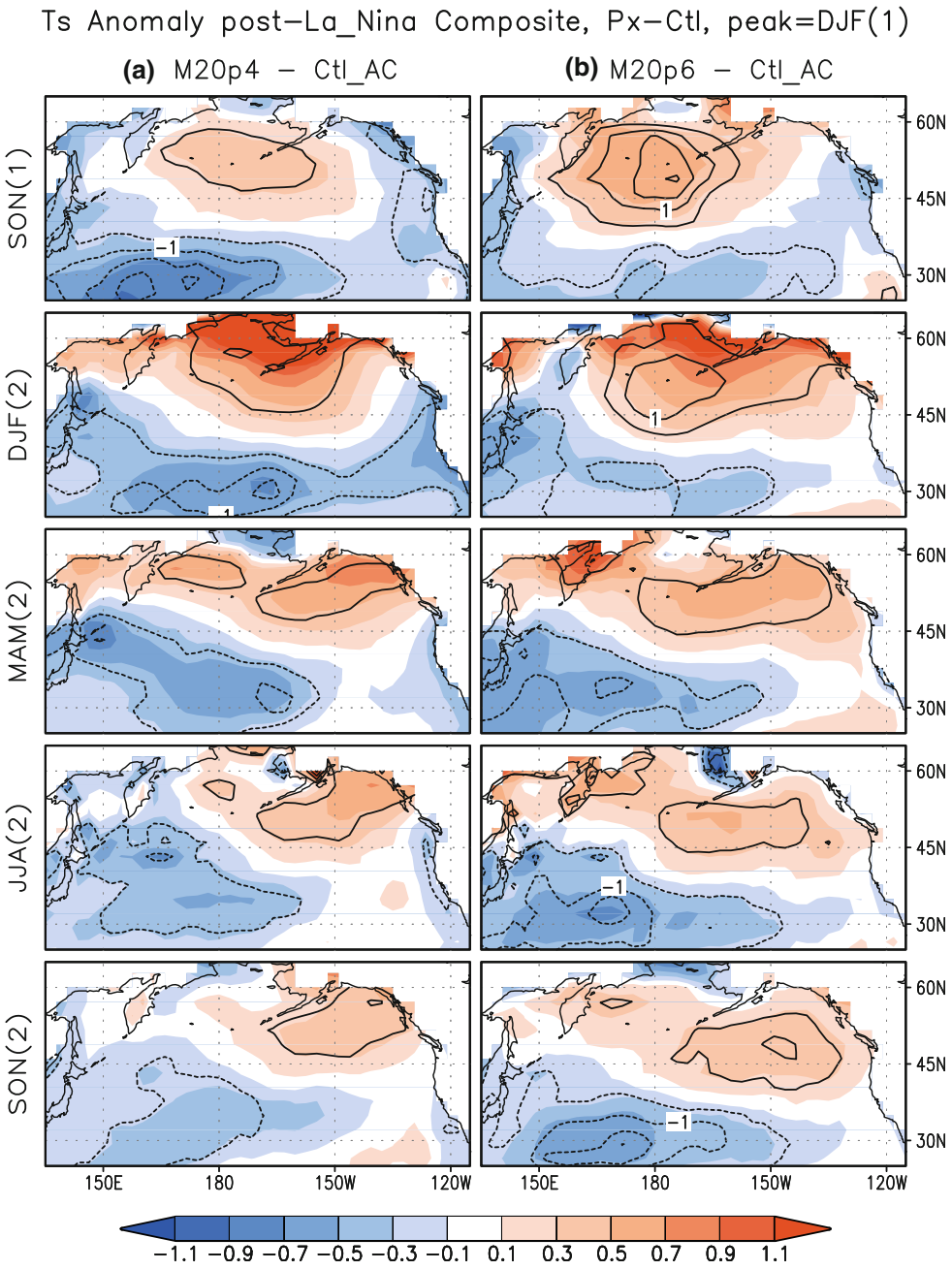

Fig. 9 Same as Fig. 7, but for 1 year after La Niña. The peak of La Niña was in December–February in previous year (DJF(1))

ENSO dominates local forcing, it is expected that pattern similarity will increase in every ENSO event. Moreover, we can examine how long the similarity of ENSO response pattern persists. Second, we will perform variance analysis based on the hypothesis that local forcing is independent of remote forcing.

4.1 ENSO response pattern similarity

Here the pattern similarity is defined by spatial correlation score and spatially root-mean-squared anomaly difference between any two events in the North Pacific basin. The North Pacific domain is defined as 152°E–132°W in longitude, and 32–54°N in latitude, and seasonal mean is calculated by 3-month running mean. For the null hypothesis, the result of control experiment is used (i.e., local forcing only). In detail, because there are 60 years of control experiment simulation, if we choose any two years for comparing the same seasonal mean pattern, 1770 ($=_{60}C_2$) pairs are possible for the calculation. In the same way, for the ENSO experiments, 435 ($=_{30}C_2$), 105 ($=_{15}C_2$), and 45 ($=_{10}C_2$) pairs are the sample size in the P2, P4 and P6 experiment, respectively. Figures 10 and 11 show all samples average and standard deviation of spatial correlation (SCORR) and root-mean-squared anomaly differences (RMSD) for the surface temperature (Ts) and surface latent plus sensible heat flux (LHF + SHF).

Before starting discussion for the pattern similarity, we need to note the strong seasonality of RMSD. The RMSD of Ts and LHF + SHF in Figs. 10 and 11 has own annual cycle which looks similar between the control and ENSO experiments. This seasonality of RMSD is related to the magnitude of local atmospheric forcing (i.e., internal atmospheric dynamics). In Figs. 10h, and 11h, the lowest RMSD value in the control experiment is seen in boreal fall for Ts, and boreal summer for LHF + SHF. The reason why the value is the smallest in these seasons is not because the pattern become similar each other, but because overall magnitude of anomalies decrease in these seasons. We calculated spatially root-mean-squared anomaly of Ts and LHF + SHF in the same North Pacific domain in the control experiment, and the seasonal evolution of spatial mean magnitude of anomaly is same as Figs. 10h and 11h, respectively (not shown). This result suggests an annual cycle where local atmospheric forcing in the winter season increases the variability of surface heat flux. The increased variability of Ts is one season delayed. After the spring season, large magnitude of Ts anomaly is damped out through the fall season. This annual cycle is so strong that general fluctuation is mostly maintained without respect to the remote forcing.

The tropical El Niño forcing results in significantly increased SCORR of Ts (Fig. 10b–d). In all ENSO experiments, mean SCORR of Ts El Niño responses the peak of which is in boreal spring are higher than the La Niña responses. Thereafter, the similarity decreases and become insignificant in following winter. This result indicates that the Ts lingering pattern of El Niño response is not statistically significant, supporting previous result in the Sect. 3.2. In the case of P2 experiment, the mean SCORR of Ts is lower than those in the P4 or P6 experiment, consistent with the weak normalized signal in the composite analysis. Both the P4 and P6 experiments show mean SCORR of Ts El Niño response over 0.3, but the RMSD results suggest that the P6 experiment simulates more consistent ENSO responses. Comparing Fig. 10e with 10f after the El Niño peak season, the RMSD of Ts is significantly reduced in the P6 experiment, but not in the P4 experiment. This result can be translated to that pattern structures are similar, but magnitude of anomalies are variable event-by-event in the P4 experiment.

In Fig. 11, the SCORR of LHF + SHF is consistent with Ts result. A sharp peak over 0.3 in the El Niño peak season in the P6 experiment, which means more consistent heat flux deriving Ts evolution, supports the previous results of high Ts SCORR and low Ts RMSD. In the P4 experiment, the SCORR in the El Niño peak season is significantly high, but looks stubby. Relatively high SCORR of LHF + SHF in the summer season (around JJA(1)) in all ENSO experiments suggests that the structure of negative air–sea feedback which damps the large magnitude of Ts anomaly is also similar event-by-event.

The La Niña responses are different from the El Niño responses. The average SCORR of Ts does not form a peak after the La Niña peak season (Fig. 10b–d). The maximum value is lower than the El Niño events, but significant signals persist into the subsequent year. In the P2 experiment, the mean SCORR of Ts decreases after the La Niña peak season. This might be due to the weak La Niña responses of Ts as shown in Fig. 5a. Both the P4 and P6 experiments show similar evolution of mean SCORR of Ts after the La Niña peak season. In Fig. 10d, the P6 experiment suggests that the event-by-event similar Ts patterns continue 2 years, but do not overcome the second winter season. In the P4 experiment (Fig. 10c), the La Niña response pattern similarity continued to the subsequent El Niño onset season. The increased variability of El Niño response anomaly in the P4 experiment mentioned above might be related to the La Niña responses not dissipated yet.

In the case of LHF + SHF, there is a peak of SCORR before the La Niña peak season in the P4 experiment (Fig. 11c), but no significant signals are detected in the P6 experiment (Fig. 11d). The consistent heat flux before the La Niña peak season is corresponding to the high SCORR

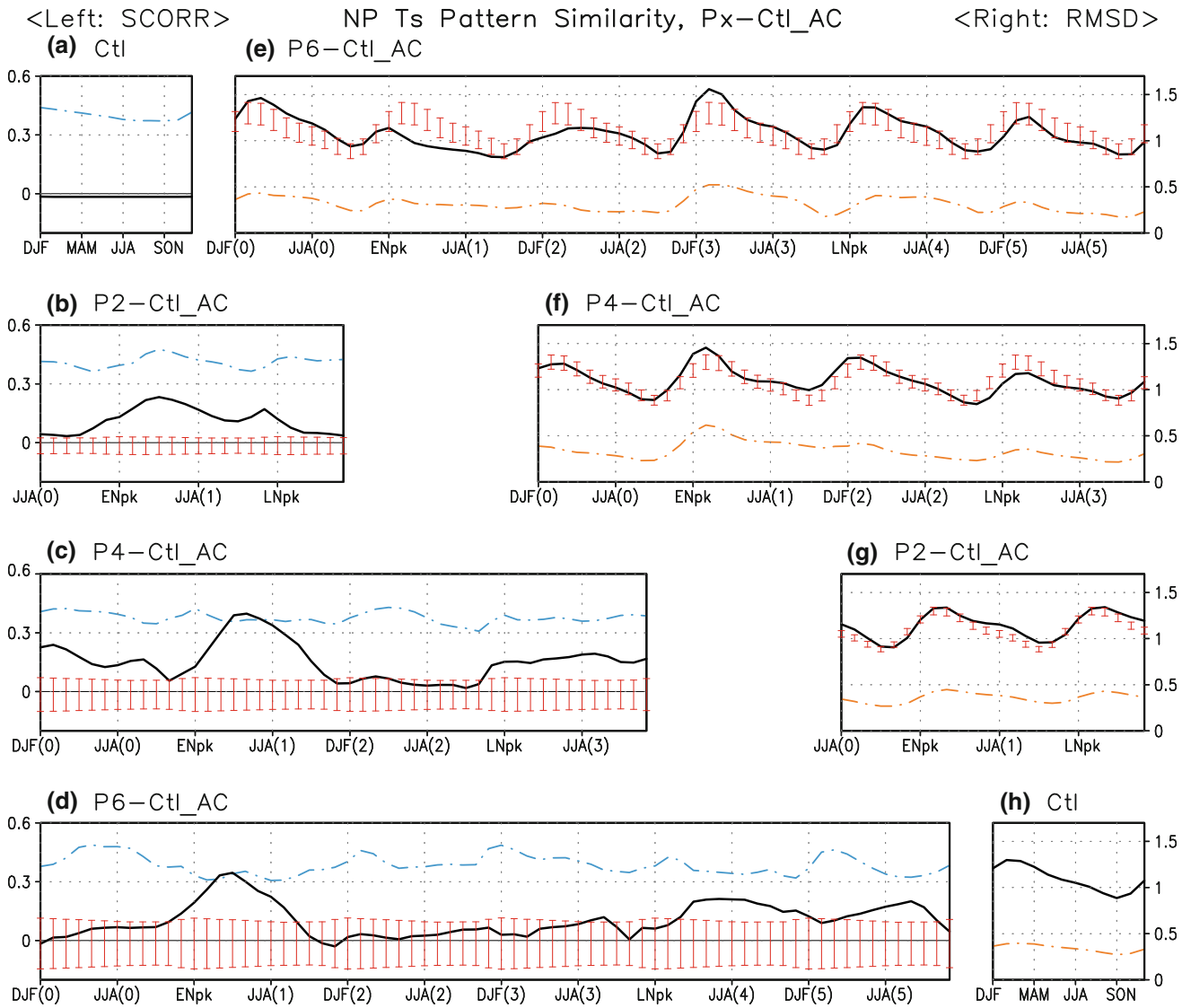

Fig. 10 Sample average (*solid line*) and standard deviation (*dot dash line*) for the spatial correlation score (SCORR, **a**–**d**) and spatially root-mean-squared anomaly difference (RMSD, **e**–**h**) in the case of surface temperature in the North Pacific domain (152°E–132°W, 32–54°N). Total 1770 ($=_{60}C_2$) pairs are used in the control (**a** and **h**), 435 ($=_{30}C_2$) pairs are in the P2 (**b** and **g**), 105 ($=_{15}C_2$) pairs are in the P4 (**c** and **f**), and 45 ($=_{10}C_2$) pairs are in the P6 experiment (**d** and **e**). *Red bar* indicates two-tailed 95% significance level range from the control experiment average for the given standard deviation of ENSO experiment. The number of degrees of freedom is 2,203, 1,873, and 1,813 for the P2, P4 and P6 experiment, respectively

of Ts from the La Niña peak season in the P4 experiment. The late increase of Ts SCORR in the P6 experiment can be explained by temporally or spatially variable heat flux responding to the La Niña forcing. Actually in the P6 experiment, both RMSD of Ts and LHF + SHF in winter before La Niña (DJF(3) in Figs. 10e and 11e) are significantly large. This variability may cause irregular heat flux response to La Niña, but the reason of abrupt large variance around DJF(3) is uncertain.

Lastly, it is worth noting that the pattern similarity of Ts ENSO responses between the P4 and P6 simulations is nearly identical with the evolution of mean SCORR in Fig. 10c or d (not shown). Because there are 15 and 10 ENSO events in the P4 and P6 experiment, respectively, we tested 150 pairs for the spatial correlation of Ts. As a result, the higher peak of mean SCORR (over 0.3) after the El Niño peak season, and rapid descent thereafter is same. The lower but flat SCORR persists through the second year is also same to the results in the P4 or P6 experiment. This result suggests that the ENSO response pattern and evolution of it in the P4 and P6 experiments are qualitatively same, and reliable.

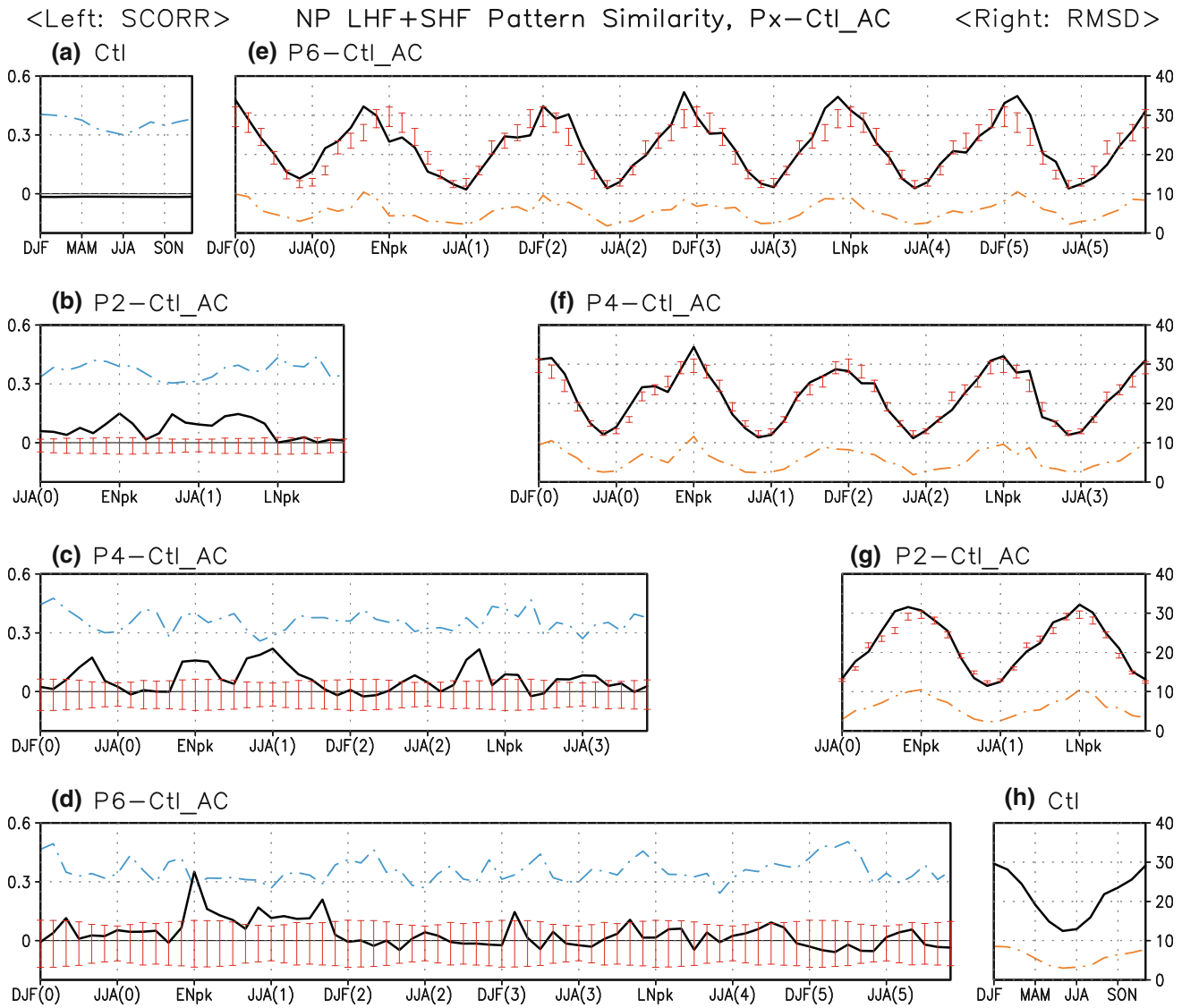

Fig. 11 Same as Fig. 10, but for the surface latent plus sensible heat flux

4.2 Independence of local and remote forcing

In addition to the event-by-event steadiness of the ENSO responses, we are also interested in the relationship between the tropical remote forcing and local variability in the North Pacific. In order to assess the statistical significance of the effect of remote forcing we performed *F* tests on the variance of surface temperature. Because Ts response to ENSO matures in the boreal spring season, we focus on this season. First, the climatological variability of the ENSO experiments is tested against the control experiment (Fig. 12a). We expected the ENSO experiment climatology to be of more variance than the control experiment due to the effect of tropical remote forcing. However, the 90% statistically significant signals are rarely detected. The blue shading, which means the variability of the ENSO experiment is bigger than that of the control experiment, is shown in the P2 experiment in the limited region. In the P4 and P6 experiments, in contrast to our expectation, most signals look noisy. The tropical remote forcing has little impact on the overall variance especially in the case of the longer ENSO period experiments. There are two possible interpretations of this result: (1) the remotely forced variability is small compared to the variability due to local processes or (2) the remote forcing somehow decreases the local variability (i.e., destructive interference).

We have also compared the ENSO composite variance to the climatological variance of the control experiment. This comparison can test which interpretation is more appropriate between two possible explanations above. If the local variability is independent of the ENSO forcing

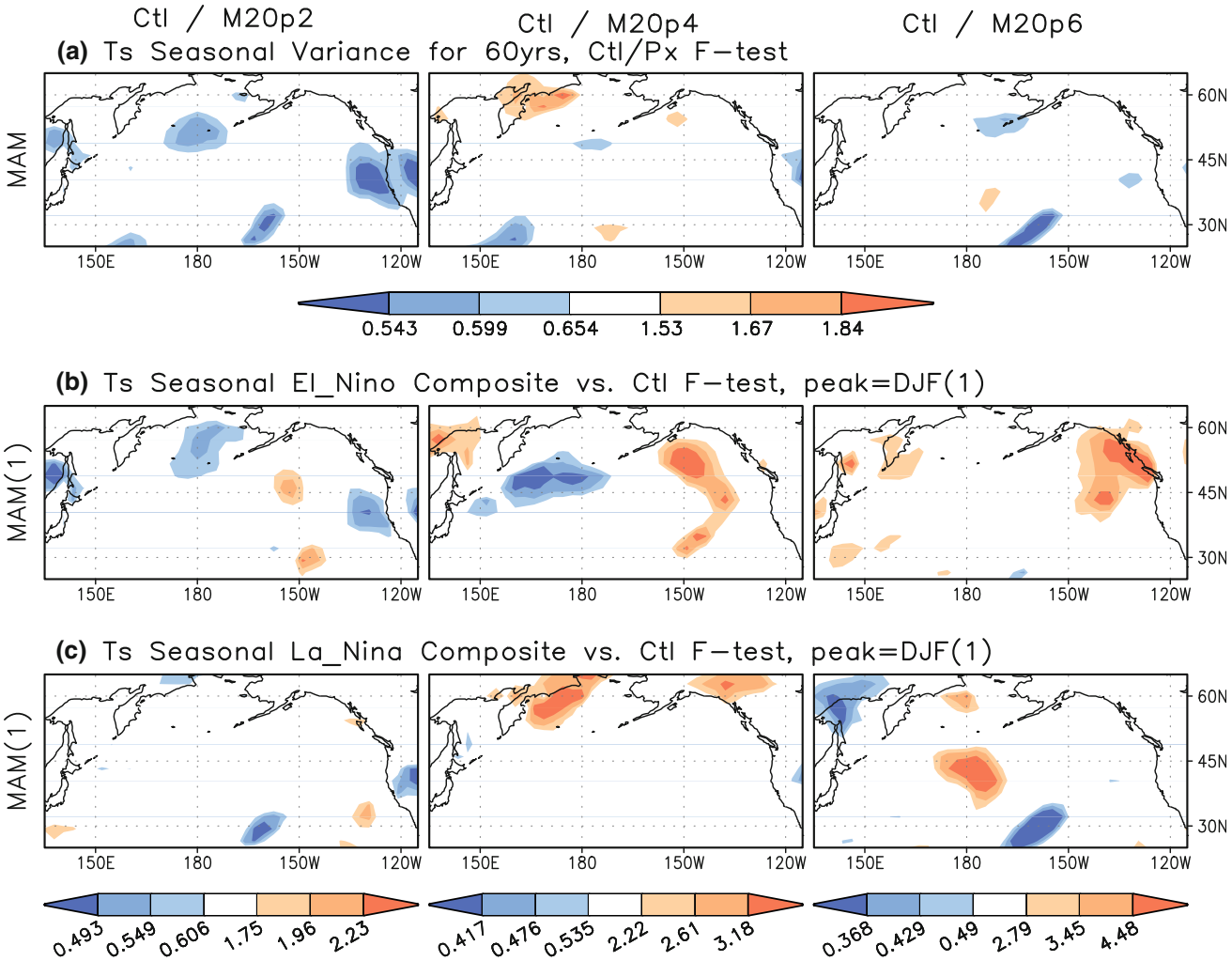

Fig. 12 *F*-test of boreal spring season surface temperature variance between the control experiment and P2 (*left column*), P4 (*middle column*), and P6 (*right column*) experiment. (**a**) The variance for entire 60 years (climatology), (**b**) the control experiment for 60 years to the P2, P4, and P6 experiment El Niño composite, and (**c**) the control experiment for 60 years to the P2, P4, and P6 experiment La Niña composite. *Each level* indicates two-tailed 90, 95, and 98% significance level based on the number of degrees of freedom, (**a**) (59, 59), and (**b**, **c**) (59, 29), (59,14), and (59,9) for the P2, P4, and P6 experiment, respectively

(i.e., the remote forcing does not decrease the local variability), we expect the difference between the ENSO composite variance and control experiment climatology to be statistically insignificant. Fig. 12b, c show the ratio of surface temperature variance in the control experiment for 60 years to those in the ENSO experiments for the El Niño or La Niña composite, respectively. In Fig. 12b, c, signals over the 90% significance level clearly appear although they are limited in spatial extent. In the case of the P2 and P4 experiments El Niño composites, the variance in the northern central North Pacific is significantly increased compared to the control experiment (Fig. 12b, shown as blue shading). On the other hand, there also exists significantly reduced variance in the ENSO experiment. In the case of P4 and P6 experiment El Niño composite, red shading is seen in the northeastern North Pacific (Fig. 12b). In the La Niña composite, red shading also appears in the central North Pacific in the P6 experiment (Fig. 12c). These results support the notion that the local variability is not independent of the tropical remote forcing specifically in the longer period ENSO experiment. The tropical remote forcing can increase or decrease local variability depending on the region, and the destructive or constructive interference associated with the remote forcing is stronger in the El Niño composite than in the La Niña composite.

5 Comparison to the observation

The numerical experiments in this study showed that the surface temperature El Niño responses in the North Pacific

are more robust and consistent than the La Niña responses. In the aspect of "persistence," however, significant similarity of La Niña responses reaches in subsequent year while the El Niño responses rapidly diverge after maturing season. These characteristics in the model results are compared to the observation.

In the observational estimates data, because temporal and spatial evolution of ENSO is not uniform, and available samples are limited, it is impossible to compare the effects of different periodicity. In this section, we will only examine the composite of nine El Niño and La Niña events which are presented in Table 1. In addition, it is also unfeasible to distinguish the "no ENSO years" like the control experiment. Hence, we used all years (1948–2005) except for the ENSO composite years as the control (hereafter "Obs Control").[4]

Similar to the previous model composite analysis, seasonal evolution of the North Pacific ENSO responses are displayed in Fig. 13. Comparing Figs. 4 and 5 with Fig. 13, first, spatial structure is different, specifically in the La Niña events. The La Niña responses in the numerical model were northern positive and southern negative dipole pattern. In the observational estimates, the La Niña response pattern is more symmetric to the El Niño response pattern with opposite sign. The symmetric pattern is most apparent in the boreal spring season, one season after the ENSO peak season, although the magnitude of anomaly is larger in the La Niña composite.

Second, we have previously noted that the numerical model simulates larger magnitude of surface temperature anomaly in responding to El Niño than La Niña. In nature, Fig. 13 shows that the La Niña responses are stronger than the El Niño responses. In the La Niña responses, large magnitude of normalized anomaly in the central North Pacific is already seen before the La Niña peak season (Fig. 13b top panel). Thereafter, anomaly composite more than 0.7°C is maintained into the subsequent boreal spring season. In contrast, the El Niño response in the boreal winter season is weakened, and longitudinal extent of which is stretched eastward, compared to the previous fall season. Consequently, in the following spring season, the El Niño response mature pattern is weaker than the La Niña response.

Lastly, maximum responses in the experimental results appear in boreal spring to summer. In Fig. 13, the maximum response pattern is also seen in the boreal spring season. However, after spring, the response pattern is changed (Fig. 13a bottom panel) or dissipated (Fig. 13b bottom panel). It is also worth noting that the ENSO composite pattern in the observational estimates is already clear in the boreal fall season, one season before the ENSO peak season, while that in the experiments was indistinct yet.

The stronger composite pattern in the fall season is also supported by the pattern similarity analysis. As similar to the Fig. 10, Fig. 14 shows mean and standard deviation of SSTA SCORR and RMSD. Here, 36 ($=_9C_2$) pairs of El Niño or La Niña composite are compared to the 780 pairs in Obs Control ($_{40}C_2$). As consistent with the previous composite pattern result, La Niña composite patterns are of higher SCORR and less RMSD after the La Niña peak season, while the SCORR around El Niño peak season is not significant. In the both El Niño and La Niña composite (Fig. 14b, c), there is one more peak before the ENSO peak season. This suggests that, in nature, the effect of tropical remote forcing affects the North Pacific from the ENSO onset season. In addition, abrupt descent of La Niña response SCORR after the boreal spring season suggests that the damping process is more effective in nature than the slab mixed layer ocean model coupled to the AGCM. After the boreal summer, two seasons after the ENSO peak season, the SCORR in both Fig. 14b and c is nearly zero, so there is no clue for the lingering pattern. It is also different from the model results that the maximum RMSD appear in late summer, not in the winter season. Spatially root-mean-squared magnitude of anomaly is also the largest in the late summer season (not shown). This indicates that the local forcing deriving more variability of SST exists in (early) summer season. This local forcing may be responsible for the rapid dissipation of La Niña response anomalies.

As similar to the Fig. 12, the variance analysis is also performed for the observational estimates (Fig. 15). Here, the variance of NINO3.4 is also analyzed because the evolution of NINO3.4 in each ENSO event is not identical in nature. The NINO3.4 variance comparison indicates that the composite variance around the ENSO peak season is not distinguished significantly from the Obs Control. However, the *F* test in the North Pacific indicates that the ENSO composite is of less variance than the variance of Obs Control in the limited region (red shading in Fig. 15c, d). This result is similar to the result in the longer ENSO period experiments, supporting the suppressed local forcing by the remote forcing, although the region of red shading is different each other. In addition, the t-test result (contour in Fig. 15c, d) shows larger significant region in the La Niña composite, consistent with previous composite mean pattern result. In the La Niña composite, the significant *t* test signals largely co-exist with the significant *F* test signals, so we need to be careful to interpret the *t* test result.

[4] From the total 58 years (1948–2005), 18 ENSO composite years are excluded, so the length of Obs Control is 40 years. Excluded ENSO year is 12 months from Jun in previous year (year 0) to May in subsequent year (year 1), which is based on the NINO3.4 composite evolution shown in Fig. 15a.

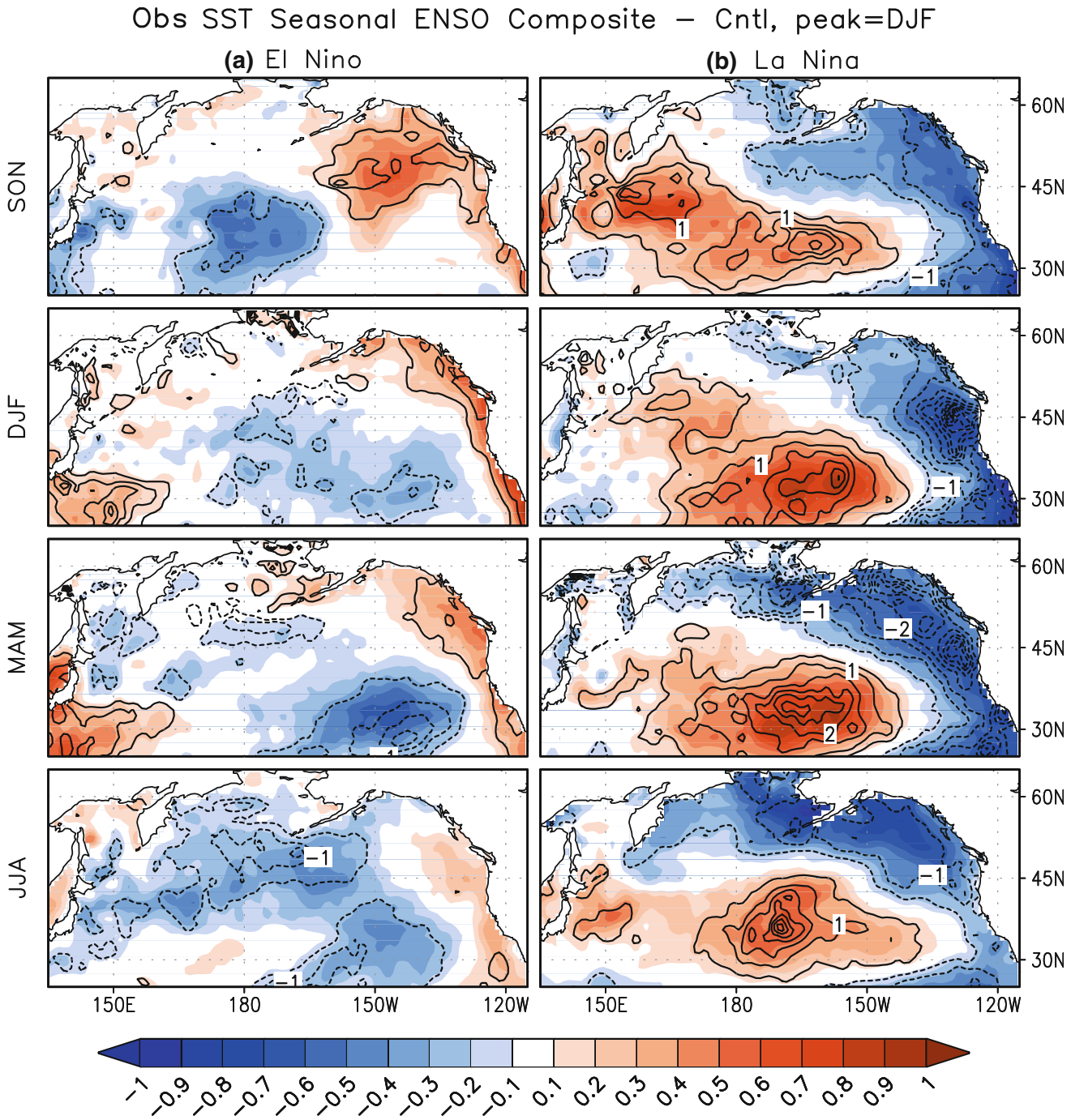

Fig. 13 Seasonal sea surface temperature anomaly (SSTA) composite (*shading*, °C) and standardized composite (*contour*) in the (**a**) El Niño and (**b**) La Niña events for the Hadley Centre dataset. Each nine El Niño and La Niña years for the composite are presented in Table 1. The peak of ENSO is in December–February, second panels from the top. The standardization is calculated by dividing the anomaly composite with the standard deviation of the anomaly used in the composite analysis. *Solid line* indicates positive, and *dash line* indicates negative values. *Zero line* is suppressed. Contour level is 0.5

6 Changed seasonal climatology

Previously we argued that the existence of variability in the tropical Pacific causes changes in seasonal climatology in the North Pacific. In this section, the changed climatology is examined in detail. First, we need to test whether the change in the climatology is statistically significant or not. Fig. 16 shows the results of a *t* test between the ENSO experiments and the control experiment. In Fig. 16, all four seasons of each ENSO experiment is consistently significantly different at the 99% confidence level. The pattern of significant signal is different among the experiments, but independent of the season.

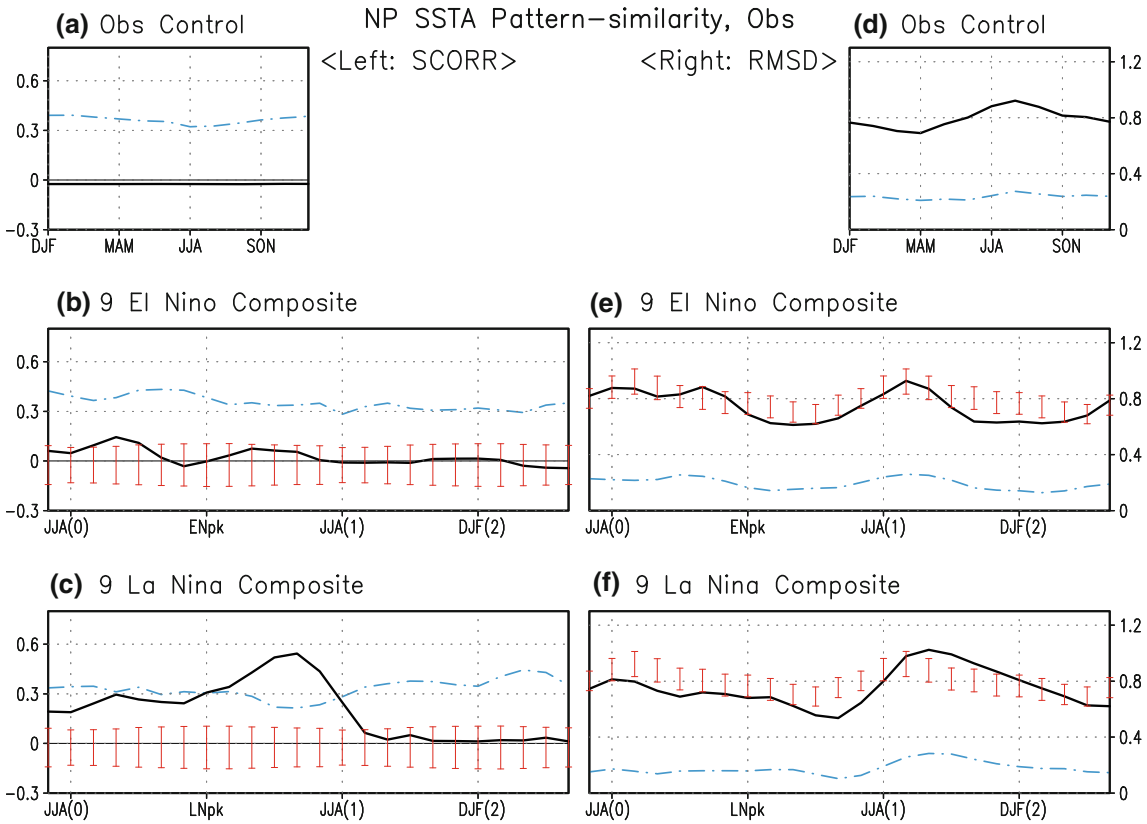

Fig. 14 Sample average (*solid line*) and standard deviation (*dot dash line*) for the spatial correlation score (SCORR, **a**–**c**) and spatially root-mean-squared anomaly difference (RMSD, **d**–**f**) in the case of sea surface temperature in the North Pacific domain (152°E–132°W, 32–54°N). Total 780 ($=_{40}C_2$) pairs are used in Obs Control (**a** and **d**), 36 ($=_9C_2$) pairs are for the El Niño (**b**, **e**) and La Niña (**c**, **f**) composite. *Red bar* indicates two-tailed 95% significance level range from the Obs Control average for the given standard deviation of ENSO composite. The number of degrees of freedom is 814

The *t* test result in Fig. 16 generally indicates negative anomalies in mid-latitude west-to-central North Pacific, and positive anomalies in the high-latitude central North Pacific. The patterns seen in Fig. 16 are reminiscent of a combination of El Niño and La Niña responses. Thus it is hypothesized that the change in the climatology is caused by the ENSO forced pattern. Because the same ENSO event repeats in the tropical Pacific, the similar ENSO forced pattern may also repeat in the North Pacific, and the repeated pattern could project onto the climatology.

To test this hypothesis, the seasonal climatology is compared to the averaged composite of El Niño and La Niña. Figure 17 shows the result of the P4 experiment, the anomalies of which are from the control experiment annual cycle. The shaded patterns in the left and right panels are similar to each other. The spatial correlation coefficient has also been calculated (Table 4). The correlation indicates over 94% pattern similarity during all seasons. In the case of P6 experiment shown in Fig. 18, the pattern correlation in all seasons except boreal fall is over 95%. In the boreal fall, the similarity is just below 90%.

Previously we argued that the El Niño and La Niña forced patterns are well balanced in the sense of anomaly magnitude when the anomaly composite is calculated from its own annual cycle, but they are not balanced when the anomaly composite is from the control experiment annual cycle. As noted here, the climatologies in the various experiments differ from each other and the control. The differences in the annual cycle between the ENSO and control experiments are similar to the ENSO forced pattern. Consequently, the annual cycle of each ENSO experiment already contains the characteristics of the ENSO forced pattern compared to the control experiment. This is why Fig. 3 shows quite linear ENSO response signals with opposite sign.

7 Summary and conclusion

The effect of ENSO frequency on the North Pacific has been examined. In nature, because the frequency of ENSO is not fixed, it is hard to examine the effect of ENSO frequency with observational data. The experimental design

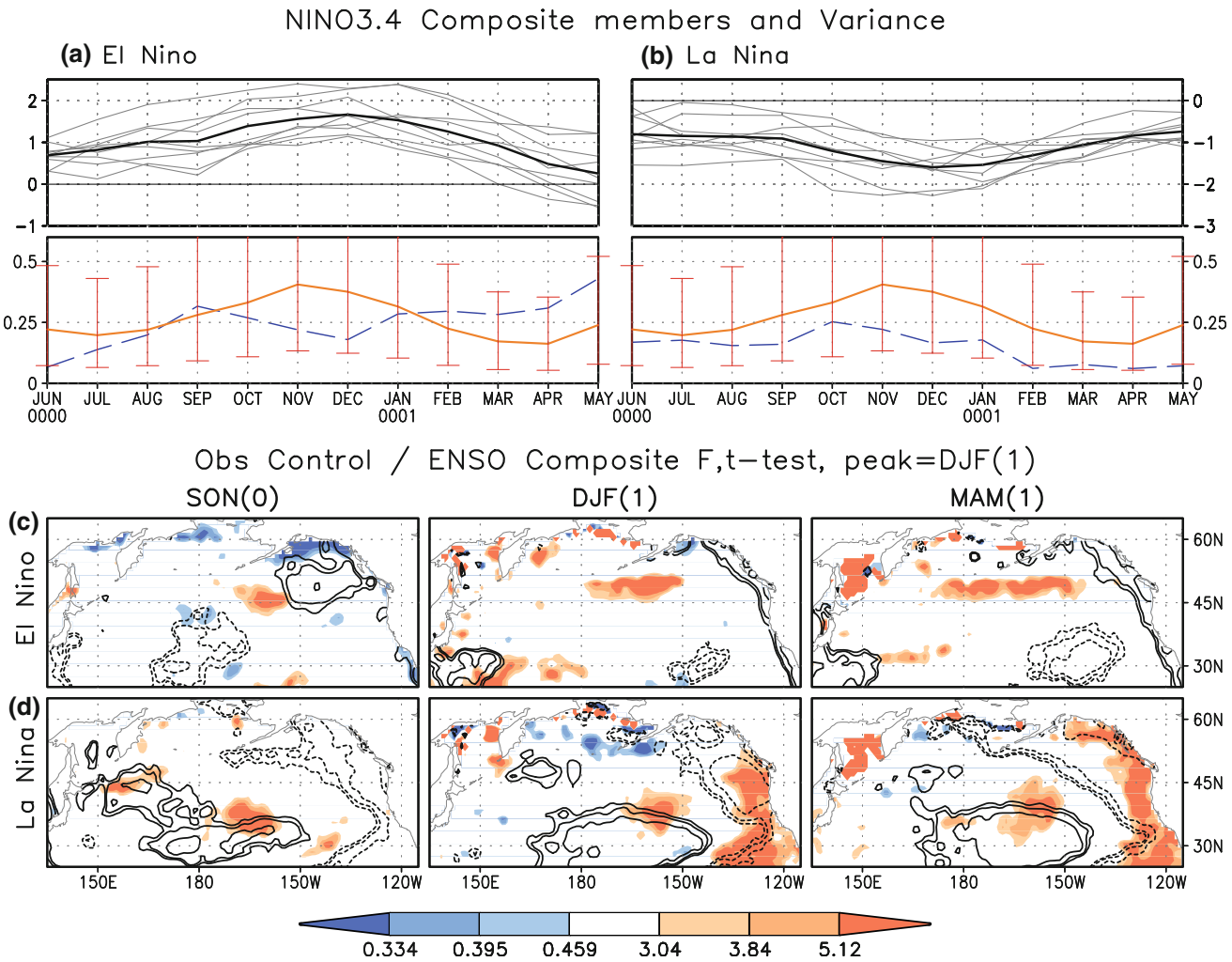

Fig. 15 NINO3.4 composite member (*gray thin solid line*), composite mean (*black thick solid line*), Obs Control NINO3.4 variance (*orange solid line*), and variance of composite members (*blue dash line*) are shown for (**a**) El Niño and (**b**) La Niña. Red bar indicates two-tailed 90% (one-tailed 95%) significance level variance range from the all year variance based on the number of degrees of freedom, (39.8). In addition, *F*-test (shading, Obs Control/ENSO composite) and *t* test (contour, ENSO composite–Control) of SST in boreal fall to spring season between Obs Control and (**c**) nine El Niño or (**d**) nine La Niña composite in the North Pacific basin. *Each level* indicates two-tailed 90, 95, and 98% significance level based on the number of degrees of freedom, (39, 8) for the *F*-test, and two-tailed 90, 95, and 99% significance level based on the number of degrees of freedom, 47 for the *t* test. *Solid line* indicates positive, and *dash line* indicates negative values. *Zero line* is suppressed

used in this study makes it possible to examine how a perfectly periodic ENSO affects global climate. Comparing different ENSO experiments, we analyzed the similarities and differences in surface temperature responses in the North Pacific.

The common features among the ENSO experiments are summarized as follows:

- The ENSO response in the North Pacific matures in boreal spring and summer following the peak of ENSO. The mature response pattern is maintained longer compared to the observational estimates data.
- The surface temperature response to the El Niño events consists of generally cold anomalies in the central North Pacific, and a warm anomaly along the western coast of North America compared to the control experiment annual cycle, which is similar to the observational estimates.
- The surface temperature response to the La Niña events is warm anomalies in the high-latitudes central North Pacific, which is less consistent among the ENSO experiments compared to the El Nino responses. This La Niña response pattern is totally different from that in the observational estimates.
- The response in the North Pacific is nonlinear in the sense that the El Nino composite is not perfectly out of phase with the La Nina composite.

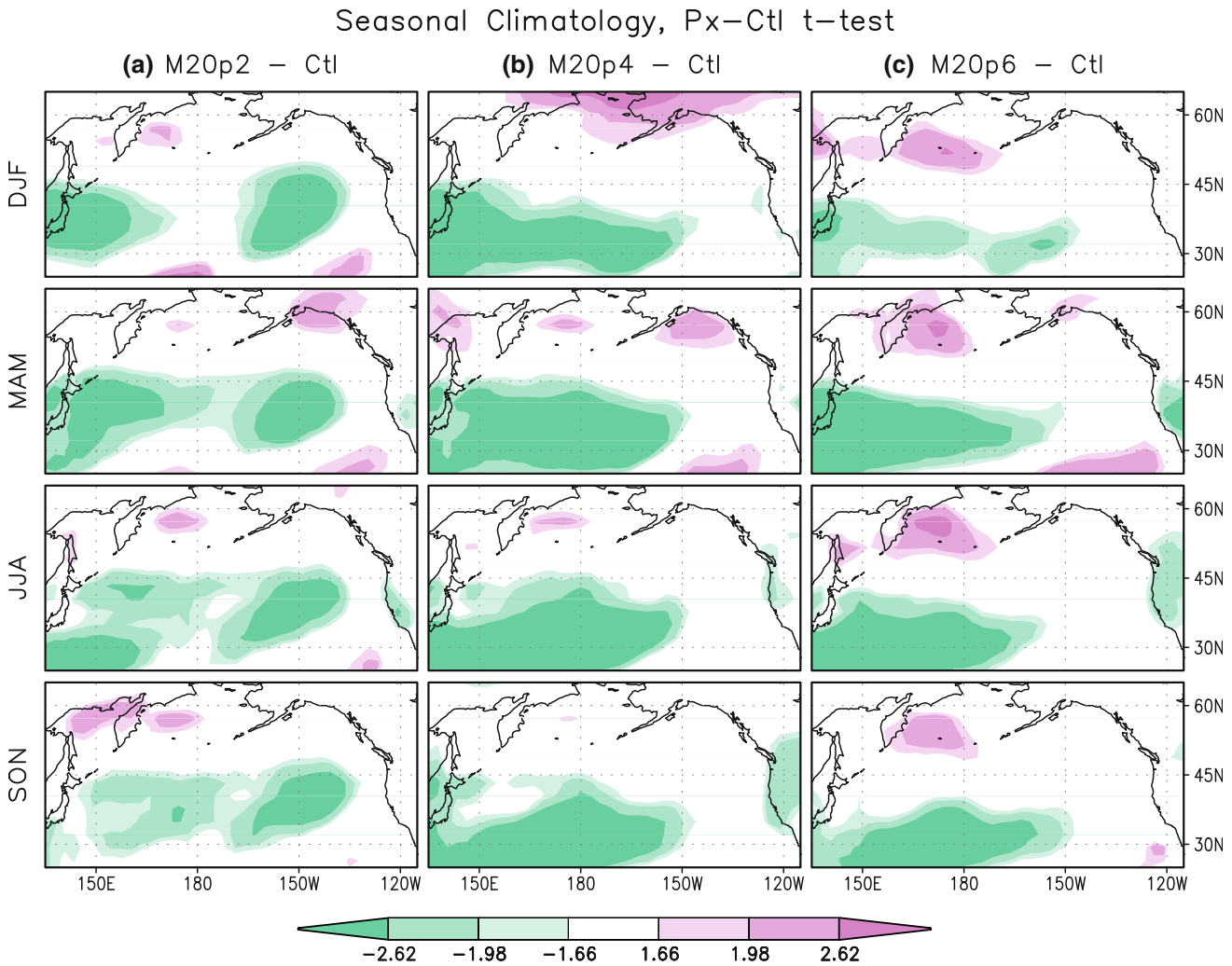

Fig. 16 Student's *t* tests of seasonal surface temperature climatology for 60 years between the control experiment and (**a**) P2, (**b**) P4, and (**c**) P6 experiment. *Each level* indicates two-tailed 90, 95, and 99% significance level based on the number of degrees of freedom, 118

- The ENSO experiments result in a shifted North Pacific seasonal climatology compared to the control experiment. The changed climatology occurs because the repeated ENSO forced signals are projected onto the climatology. The more linear response in the observational estimates than in the model results can potentially be due to the observational climatology including all ENSO events.
- In the case of the P4 and P6 experiments, the significant Ts pattern similarity of the La Niña responses persists over 1 year, while that of the El Niño responses quickly decreases after boreal summer. In nature, the ENSO responses are effectively damped in the summer season, earlier than the experimental results.

The features that make the P2 experiment distinguishable from the other longer ENSO period experiments occur because there is not enough time to damp the ENSO forced anomalies. Since an El Niño or La Niña happens every year in the P2 experiment, the residual of the previous ENSO response is superimposed onto the next year's ENSO response. This leads to relatively more variability and smaller normalized signal in boreal spring and summer when the ENSO responses mature.

The P4 and P6 experiments have one and 2 years damping time, respectively. Is this enough time to erase the traces of previous ENSO? If 1 year is enough time to damp the anomalies, then the ENSO response pattern will be similarly stable between the P4 and P6 experiments. Between the P4 and P6 experiments, the event-by-event pattern similarity (SCORR) is nearly same, but difference of anomaly magnitude (RMSD) indicates that the P6 experiment is more stable during the El Niño events. The more variability of El Niño responses in the P4 experiment is related to the previous La Niña response which is maintained through the El Niño onset season.

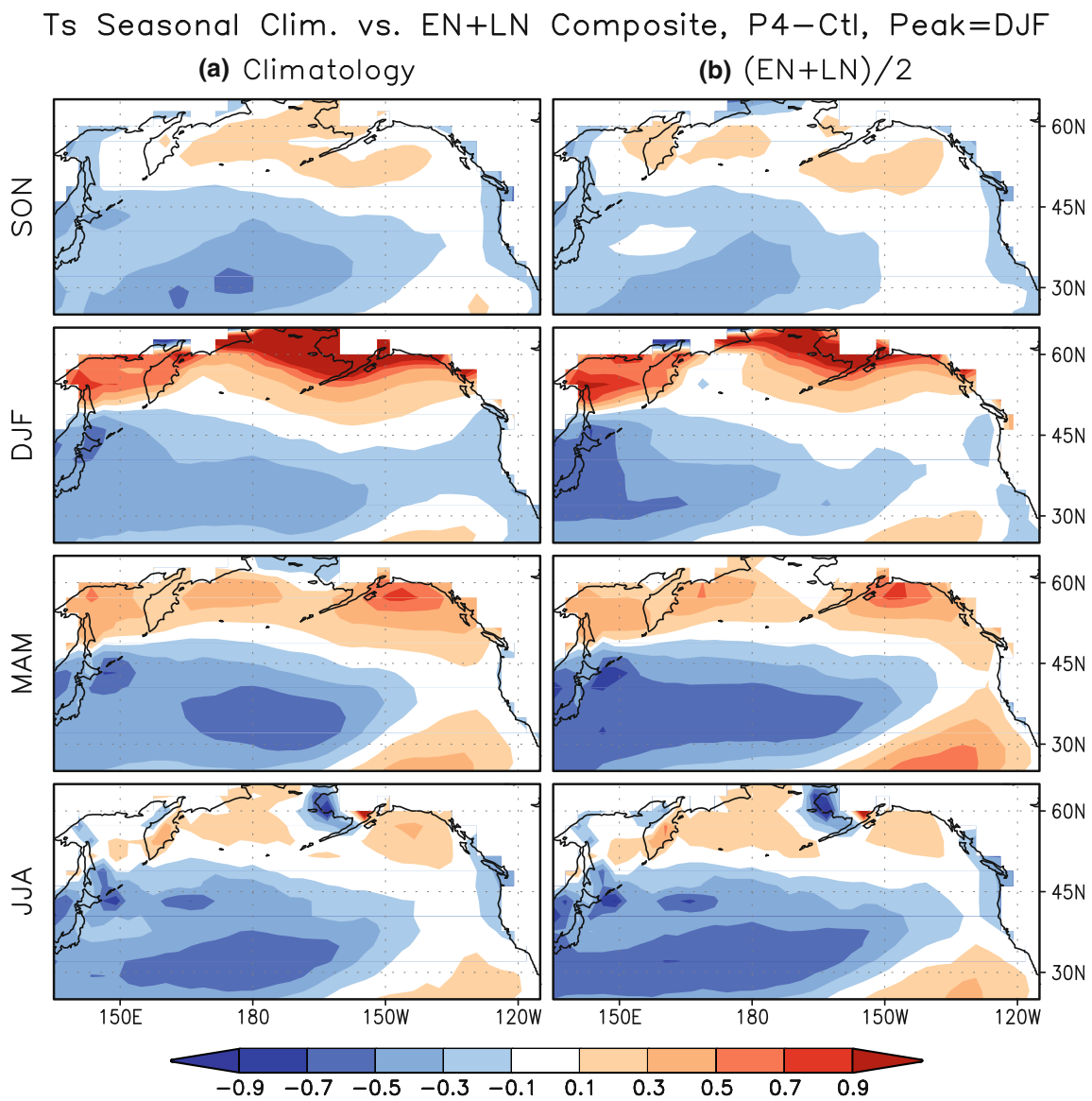

Fig. 17 Seasonal surface temperature (**a**) climatology and (**b**) averaged El Niño plus La Niña composite in the case of P4 experiment. Anomalies from the control experiment annual cycle are shown. The peak of ENSO events is in December–February, right second panel from the top

Table 4 Spatial correlation between the climatology and averaged El Niño plus La Niña composite in the case of P4 and P6 experiment, calculated in 145°E–125°W, 30–60°N

Season	P4 Exp.	P6 Exp.
September–October–November	0.953	0.895
December–January–February	0.941	0.957
March–April–May	0.957	0.964
June–July–August	0.979	0.954

In addition, we examined whether the variance by local noise is independent of the variance by tropical remote forcing. If both are independent of each other, the variance of the ENSO composite will be not significantly different from the variance of the control experiment. The *F*-test indicates that significantly different variances are seen although this is limited to specific regions. Generally, the longer the ENSO period is, the less the composite variance is. Decreased composite variance means that the ENSO forced signals suppress local variability. This phenomenon is also seen in the observational estimates although the region of significant *F*-test signal is different each other. Hence we can infer that the interfering effect of tropical remote forcing with the local variability is closely related to the local damping time and the ENSO frequency.

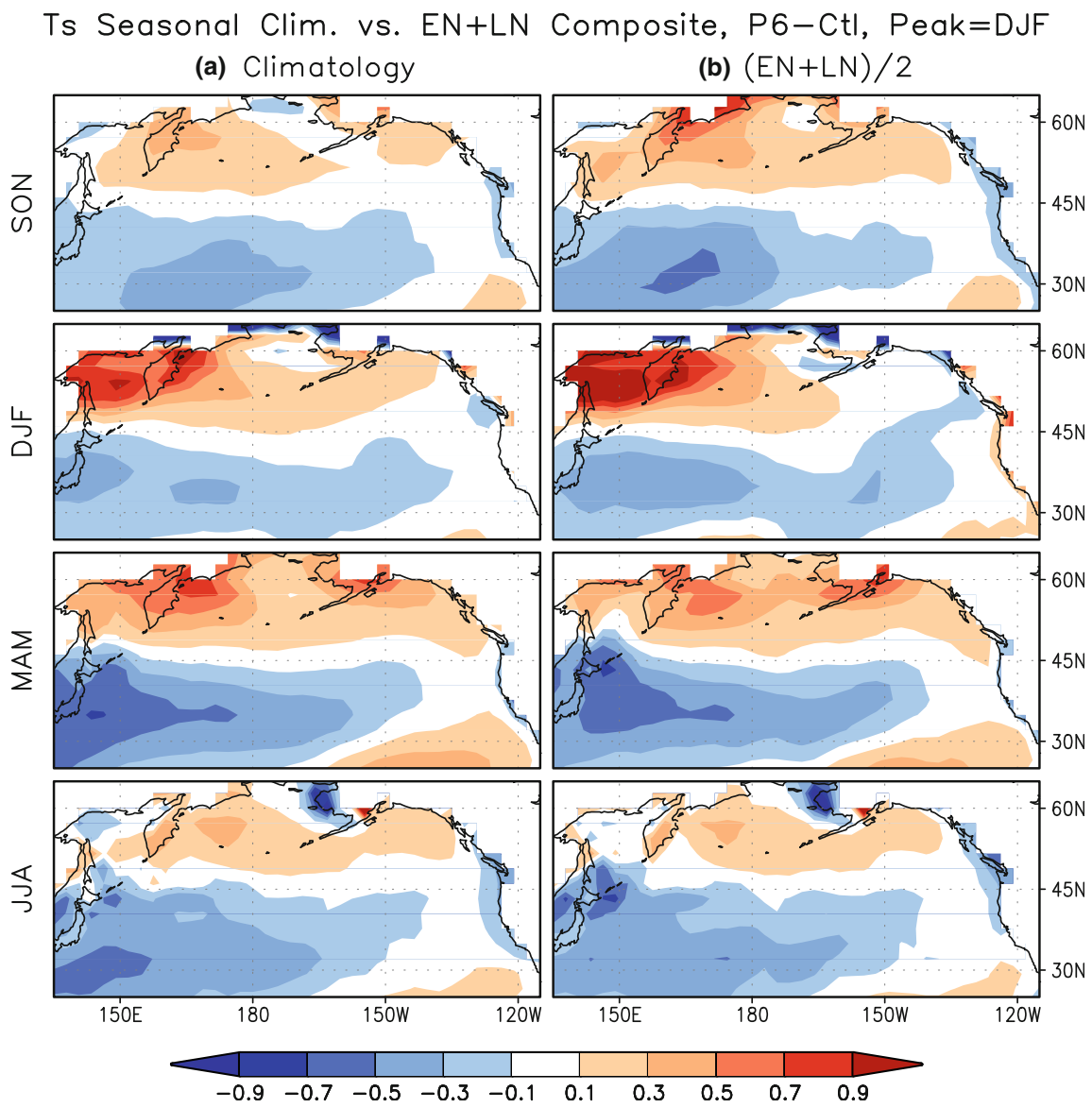

Fig. 18 Same as Fig. 17, but for the P6 experiment

Acknowledgment This manuscript is a part of George Mason University PhD dissertation of DJ. DJ would like to thank dissertation committee members, Professor Tim DelSole, Edwin Schneider, and David Straus for comments and suggestions improving the manuscript. We also thank two anonymous reviewers for improving the first draft of this paper. BPK acknowledges support from NOAA grants NA17RJ1226 and NSF grants OCI0749165 and ATM0754341.

Appendix

Statistical significance of spatial correlation

Here we present an additional calculation addressing the statistical significance of correlation coefficients shown in Table 3. In Table 3, the spatial correlation coefficient of the seasonal ENSO composite is calculated for entire 60-year record. The ENSO composite pattern is made from the average of 30 El Niño and La Niña events in the P2 experiment, 15 ENSO events in the P4 experiment, and 10 ENSO events in the P6 experiment. In order to support the results shown in Table 3 and exclude any sampling issues, we calculated the correlation coefficients based on a sub sampled, 36-year periods. The 36 year ENSO composite means 18 ENSO events in the P2 experiment, 9 ENSO events in the P4 experiment, and 6 ENSO events in the P6 experiment. We chose three different sub-periods for the calculation. If we assume that the entire 60 years period is from year 1 to year 60, the first sub-period (SP1) is from

Table 5 Spatial correlation between the ENSO experiments calculated in 145°E–125°W, 30–60°N. Compared to Table 3 where correlation was calculated for entire 60 years, Table 5 shows correlation coefficients for 36 years sub-period. In detail, "SP1" represents sub-period of year 1 to year 36, "SP2" represents sub-period of year 13 to year 48, and "SP3" represents sub-period of year 25 to year 60

	Season	Sub-Period	P2 vs. P4	P2 vs. P6	P4 vs. P6
El Niño Composite Peak=DJF	Sep-Nov	SP1	0.600	0.012	0.111
		SP2	0.430	0.412	0.488
		SP3	0.477	0.133	0.768
	Dec-Feb	SP1	0.923	0.021	0.123
		SP2	0.796	0.590	0.094
		SP3	0.589	0.875	0.712
	Mar-May	SP1	0.847	0.825	0.720
		SP2	0.919	0.807	0.753
		SP3	0.915	0.766	0.778
	Jun-Aug	SP1	0.859	0.772	0.694
		SP2	0.952	0.713	0.710
		SP3	0.920	0.645	0.713
La Niña Composite Peak=DJF	Sep-Nov	SP1	0.525	0.132	0.337
		SP2	0.450	0.379	0.529
		SP3	0.429	0.304	0.585
	Dec-Feb	SP1	0.752	0.732	0.844
		SP2	0.625	0.601	0.830
		SP3	0.508	0.564	0.724
	Mar-May	SP1	0.593	0.518	0.822
		SP2	0.433	0.621	0.764
		SP3	0.472	0.718	0.588
	Jun-Aug	SP1	0.493	0.457	0.875
		SP2	0.428	0.676	0.843
		SP3	0.371	0.676	0.624

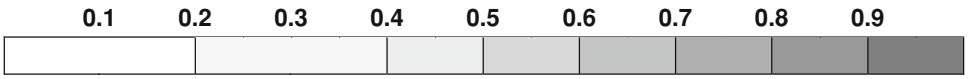

year 1 to year 36, the second sub-period (SP2) is from year 13 to year 48, and the third sub-period (SP3) is from year 25 to year 60. Table 5 displays the correlation results for the sub-periods. Comparing Table 3 with Table 5, the general trend is similar each other. In the El Niño composite, the spatial correlation between the P2 and P4 experiment is typically the highest, specifically from boreal winter to summer. In the La Niña composite, the correlation between the P4 and P6 experiment is also typically higher than the other columns. However, the details are not always similar between Tables 3 and 5. For example, Table 5 shows that the correlation in SP3 is different from those in SP1 or SP2 (e.g. P2 vs. P4 in boreal winter in the El Niño composite, P4 vs. P6 in boreal spring and summer in the La Niña composite). In summary, sub-sampled calculation of spatial correlation is generally consistent with entire period correlation although there are a few exceptions. Hence, this result strengthens the significance of Table 3.

References

An S-I, Wang B (2000) Interdecadal change of the structure of the ENSO mode and its impact on the ENSO frequency. J Clim 13:2044–2055

Collins WD, Rasch PJ, Boville BA, Hack JJ, McCaa JR, Williamson DL, Briegleb BP (2006) The formulation and atmospheric simulation of the community atmosphere model version 3 (CAM3). J Clim 19:2144–2161

Graham NE (1994) Decadal-scale climate variability in the tropical and North Pacific during the 1970s and 1980s: observations and model results. Clim Dyn 10:135–162

Hoerling MP, Kumar A, Zhong M (1997) El Niño, La Niña, and the nonlinearity of their teleconnections. J Clim 10:1769–1786

Hoerling MP, Kumar A, Xu T (2001) Robustness of the nonlinear climate response to ENSO's extreme phases. J Clim 14:1277–1293

Jin D, Kirtman BP (2009) The extratropical sensitivity to the meridional extent of tropical ENSO forcing. Climate Dyn. doi: 10.1007/s00382-009-0600-1

Kalnay E et al (1996) The NCEP/NCAR 40-year reanalysis project. Bull Am Meteor Soc 77:437–471

Kestin TS, Karoly DJ, Yano J-I (1998) Time–frequency variability of ENSO and stochatic simulations. J Clim 11:2258–2272

Kiehl JT, Hack JJ, Bonan GB, Boville BB, Williamson DL, Rasch PJ (1998) The National Center for Atmospheric Research Community Climate Model: CCM3. J Clim 11:1131–1149

Kim K-Y, O'Brien JJ, Barcilon AI (2003) The principal physical modes of variability over the tropical Pacific. Earth Interact 7(3):1–32

Kirtman BP, Shukla J (2002) Interactive coupled ensemble: a new coupling strategy for CGCMs. Geophys Res Lett 29:1029–1032

Liu Z, Alexander M (2007) Atmospheric bridge, oceanic tunnel, and global climatic teleconnections. Rev Geophys 45:RG2005. doi:10.1029/2005RG000172. http://www.agu.org/pubs/crossref/2007/2005RG000172.shtml

Rayner NA, Parker DE, Frich P, Horton EB, Folland CK, Alexander LV (2000) SST and sea-ice fields for ERA40 proceedings of the second WCRP international conference on reanalyses. World Climate Research Program, Wokefield Park, Reading, United Kingdom, pp 18–21

Toniazzo T (2006) Properties of El Niño-Southern oscillation in different equilibrium climates with HadCM3. J Clim 19:4854–4876

Trenberth KE, Hurrell JW (1994) Decadal atmosphere-ocean variations in the Pacific. Clim Dyn 9:303–319

Trenberth KE, Branstator GW, Karoly D, Kumar A, Lau N-C, Ropelewski C (1998) Progress during TOGA in understanding and modeling global teleconnections associated with tropical sea surface temperatures. J Geophys Res 103:14291–14323

Yeh S-W, Kirtman BP (2004) The impact of internal atmospheric variability on the North Pacific SST variability. Clim Dyn 22:721–732

Zelle H, Oldenborgh GJV, Burgers G, Dijkstra H (2005) El Niño and greenhouse warming: results from ensemble simulations with the NCAR CCSM. J Clim 18:4669–4683